Article

Cell Reports

Tmem160 contributes to the establishment of discrete nerve injury-induced pain behaviors in male mice

Graphical Abstract

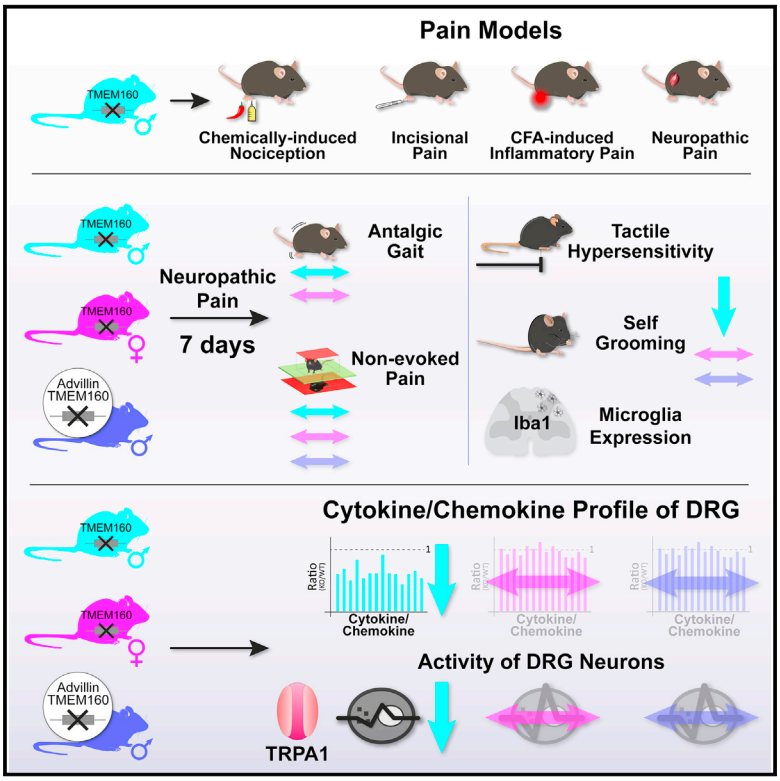

Highlights

- Discrete nerve injury-induced pain behaviors are delayed in male *Tmem160* KO mice
- Tmem160 is dispensable for other pain entities and in female KO mice
- *Tmem160* deficiency dampens neuroimmune signaling and TRPA1 activity in male DRG

Authors

Daniel Segelcke, Hanna K. Fischer, Meike Hütte, ..., Nils Brose, Esther M. Pogatzki-Zahn, Manuela Schmidt

Correspondence

manuela_schmidt@univie.ac.at

In brief

Segelcke et al. report Tmem160 as a sexually dimorphic factor contributing to the establishment, but not maintenance, of discrete nerve injury-induced pain behaviors in male mice.

Segelcke et al., 2021, Cell Reports *37*, 110152
December 21, 2021
https://doi.org/10.1016/j.celrep.2021.110152

CellPress

Cell Reports

CellPress
OPEN ACCESS

Article

Tmem160 contributes to the establishment of discrete nerve injury-induced pain behaviors in male mice

Daniel Segelcke,[1,6] Hanna K. Fischer,[5,6] Meike Hütte,[2] Sven Dennerlein,[3] Fritz Benseler,[4] Nils Brose,[4] Esther M. Pogatzki-Zahn,[1,7] and Manuela Schmidt[5,7,8,*]

[1]Department of Anaesthesiology, Intensive Care and Pain Medicine, University Hospital Muenster, Muenster, Germany
[2]Somatosensory Signaling and Systems Biology, Max Planck Institute of Experimental Medicine, Goettingen, Germany
[3]Department of Cellular Biochemistry, University Medical Center Goettingen, Goettingen, Germany
[4]Department of Molecular Neurobiology, Max Planck Institute of Experimental Medicine, Goettingen, Germany
[5]Division of Pharmacology and Toxicology, Department of Pharmaceutical Sciences, University of Vienna, Vienna, Austria
[6]These authors contributed equally
[7]These authors contributed equally
[8]Lead contact
*Correspondence: manuela_schmidt@univie.ac.at
https://doi.org/10.1016/j.celrep.2021.110152

SUMMARY

Chronic pain is a prevalent medical problem, and its molecular basis remains poorly understood. Here, we demonstrate the significance of the transmembrane protein (Tmem) 160 for nerve injury-induced neuropathic pain. An extensive behavioral assessment suggests a pain modality- and entity-specific phenotype in male *Tmem160* global knockout (KO) mice: delayed establishment of tactile hypersensitivity and alterations in self-grooming after nerve injury. In contrast, Tmem160 seems to be dispensable for other nerve injury-induced pain modalities, such as non-evoked and movement-evoked pain, and for other pain entities. Mechanistically, we show that global KO males exhibit dampened neuroimmune signaling and diminished TRPA1-mediated activity in cultured dorsal root ganglia. Neither these changes nor altered pain-related behaviors are observed in global KO female and male peripheral sensory neuron-specific KO mice. Our findings reveal Tmem160 as a sexually dimorphic factor contributing to the establishment, but not maintenance, of discrete nerve injury-induced pain behaviors in male mice.

INTRODUCTION

Pathological pain represents a disease state per se and is a broad public health problem given its high prevalence and devastating consequences for affected patients (Doth et al., 2010; Dahlhamer et al., 2018; Price and Gold, 2018; Glare et al., 2019). The severity and time course of pain-associated symptoms differ among pain entities (e.g., inflammatory pain or nerve injury-induced neuropathic pain), supporting the existence of diverse pathological processes that are poorly understood at the molecular level (Price et al., 2018). Currently, treatment options are inadequate for many patients with pain due to their limited efficacy and a substantial risk of adverse effects. Hence, additional targets are urgently needed to develop innovative therapeutic strategies (Borsook et al., 2014; Gereau et al., 2014; Price and Gold, 2018; Davis et al., 2020), particularly in the wake of the opioid crisis (Glare et al., 2019). Their development undoubtedly requires a detailed mechanistic understanding of pathological pain—an endeavor that is endorsed and promoted by recent research policies (Gereau et al., 2014; Price et al., 2018).

A major focus lies on selectively targeting the peripheral nervous system (Patapoutian et al., 2009; Dubin and Patapoutian, 2010; Vaso et al., 2014). Peripheral primary sensory neurons (PSNs), such as those of dorsal root ganglia (DRG), detect both innocuous as well as noxious stimuli and relay this information to the central nervous system (CNS). Their sensitization and persistent maladaptive input represent essential drivers of pathological pain (Dubin and Patapoutian, 2010; Vaso et al., 2014); however, mechanisms leading to peripheral sensitization are diverse (Patapoutian et al., 2009; Dubin and Patapoutian, 2010), differ among pain entities, and remain to be fully elucidated. For example, in a mouse model of neuropathic pain, pathological hypersensitivity to innocuous tactile stimulation (commonly referred to as tactile allodynia) may be triggered by alterations in the activity of TRPA1 channels (Avenali et al., 2014), Piezo2 mechanically activated channels (Murthy et al., 2018) and manifold other pathways (Costigan et al., 2009; Cobos et al., 2018). Aside from PSNs, the crucial contribution of various non-neuronal cell types needs to be considered, such as neuroimmune interactions involving central microglia and peripheral monocytes (Sorge et al., 2015; Chamessian et al., 2019).

Activation of immune cell types in the initial phase of pathological pain is accompanied by tissue infiltration, changes in protein expression profiles, and the release of pro- and anti-inflammatory mediators (cytokines, chemokines, and growth factors), all of which may perpetuate neuronal hyperactivity and thereby facilitate the sensitization processes contributing to the maintenance of pathological pain (Grace et al., 2014).

Enormous efforts have been invested, from genetics to the circuit level, to pinpoint molecules involved in pathological pain. We have recently performed an extensive proteomic screen to identify candidates associated with pathological pain in membrane fractions of mouse DRG (Rouwette et al., 2016). Within this hypothesis-generating resource, we explicitly searched for transmembrane proteins with unknown functions in pain. Among them was transmembrane protein (Tmem) 160. Previous screens have shown Tmem160 to be enriched in mouse DRG (Thakur et al., 2014), where it appears to be equally distributed across neuronal subpopulations (Usoskin et al., 2015). However, the function of Tmem160, in particular in DRG and in the context of pain, is not known.

Here, we show that global *Tmem160* deficiency (knockout [KO]) in male mice delays the establishment of tactile hypersensitivity and pain-related changes in self-grooming during neuropathic pain. Notably, Tmem160 seems to be dispensable for other nerve injury-induced pain behaviors, such as non-evoked pain and functional changes in locomotion and, in addition, for acute nociceptive, incisional, and complete Freund's adjuvant (CFA)-induced inflammatory pain regardless of the pain modality. Mechanistically, we provide evidence for Tmem160 to be implicated in controlling cytokine and chemokine levels in DRG with consequences for TRPA1-mediated nociceptive signaling. Remarkably, behavioral and mechanistic alterations are sexually dimorphic and largely specific to male *Tmem160* global KO mice. Our findings reveal Tmem160 as a sexually dimorphic player contributing to the establishment, but not maintenance, of discrete nerve injury-induced pain behaviors in male mice.

RESULTS

Tmem160 is expressed in mouse peripheral sensory neurons

Tmem160 KO mice were generated using CRISPR-Cas9-technology (Figure 1A) to study the functional relevance of Tmem160 in the context of pain. The successful global deletion of *Tmem160* was confirmed by genotyping (please see STAR Methods for details), quantitative PCR in DRG (remaining *Tmem160* transcript level in KO = 0.02% ± 0.005% of wild-type [WT] littermates; N = 6 mice/genotype), and *in situ* hybridization using RNAscope technology (Figure 1B). The latter suggested the expression of *Tmem160* transcripts across PSNs in DRG (Figure 1B) in keeping with DRG single-cell RNA sequencing (RNA-seq) data (Usoskin et al., 2015) (database: mousebrain.org [Zeisel et al., 2018]). Unfortunately, mRNA-based assays are not suitable to determine the subcellular localization of Tmem160 and commercially available anti-Tmem160 antibodies that we tested lacked specificity (data not shown). Therefore, we used immunolabeling of the Myc-tagged Tmem160 protein (Tmem160-Myc) to corroborate its subcellular localization (Figure 1C). Tmem160-Myc co-localized with mitochondrial markers in cultures of dissociated DRG neurons (Figure 1C) and HEK293T cells (Figure 1D), in agreement with previous reports (Pagliarini et al., 2008). Since Tmem160 exhibits an N-terminal signal peptide (aa 1– 45), which may suffice for mitochondrial import (MitoProt II, v1.101, https://ihg.gsf.de/ihg/mitoprot.html [Claros and Vincens, 1996]), and three predicted transmembrane domains (Figure S1A), we addressed its submitochondrial localization by carbonate extraction and hypo-osmotic swelling experiments (Dennerlein et al., 2015; Aich et al., 2018) in HEK293T cells expressing a FLAG-tagged Tmem160 protein (Tmem160-FLAG). As expected, Tmem160-FLAG was present in isolated mitochondria (Figures S1B and S1C) and resistant to high pH carbonate extraction similar to MITRAC12, a mitochondrial membrane protein, and in contrast to membrane-associated TIM44 or soluble TACO1 protein (Figure S1B). To define its submitochondrial localization in more detail, we performed a hypo-osmotic swelling assay (hypo-osmotic mitoplasts [MPs]; Figure S1C). Tmem160-FLAG only became accessible to protease treatment when the outer membrane was disrupted by hypo-osmotic swelling (MPs), similar to TIM23, a marker protein for the inner mitochondrial membrane, and in contrast to the outer membrane protein TOM20 (Figure S1C). Thus, we conclude that Tmem160 is located in mitochondria and is likely integrated into the inner mitochondrial membrane.

Tmem160 is dispensable for basal somatosensation and chemically induced acute nociception in male mice

We then set out to characterize DRG in *Tmem160* KO mice. Immunohistochemistry on DRG showed only minimal differences between KO and WT mice in terms of expression pattern and frequency of Peripherin (a marker for a subset of small unmyelinated DRG neurons) and NF200 (a marker for medium- and large-diameter myelinated DRG neurons) (Figures 2A and 2B). KO mice were healthy and fertile and displayed normal motor function (Figure 2C) regarding coordination (analyzed on a Rotarod) and locomotion (comprehensive gait analysis) as well as similar somatosensory thresholds for mechanical (tactile) and heat stimulation as WT littermates (Figure 2D).

In addition, we investigated chemically induced nociception in response to the activation of TRPV1 (by unilateral injection of Capsaicin [Caps]) and TRPA1 (by unilateral injection of mustard oil [MO]) in the hindpaw. *Tmem160* KO mice were indistinguishable from WT littermates, as both showed pronounced acute nocifensive responses to either stimulus and withdrawal responses upon tactile stimulation (tactile hypersensitivity) after Caps/MO injection (Figure 3A).

Tmem160 deficiency delays the establishment of tactile hypersensitivity in the context of neuropathic pain in male mice

We then turned to longitudinal studies in established models of different pain entities. We initially tested pain-related behaviors upon unilateral plantar incision (Pogatzki and Raja, 2003) and injection of CFA (McCarson and Fehrenbacher, 2021): neither non-evoked pain (NEP; assessed by hindpaw footprint analysis; please see STAR Methods for details) nor evoked pain (represented by hindpaw withdrawal to tactile and heat stimulation)

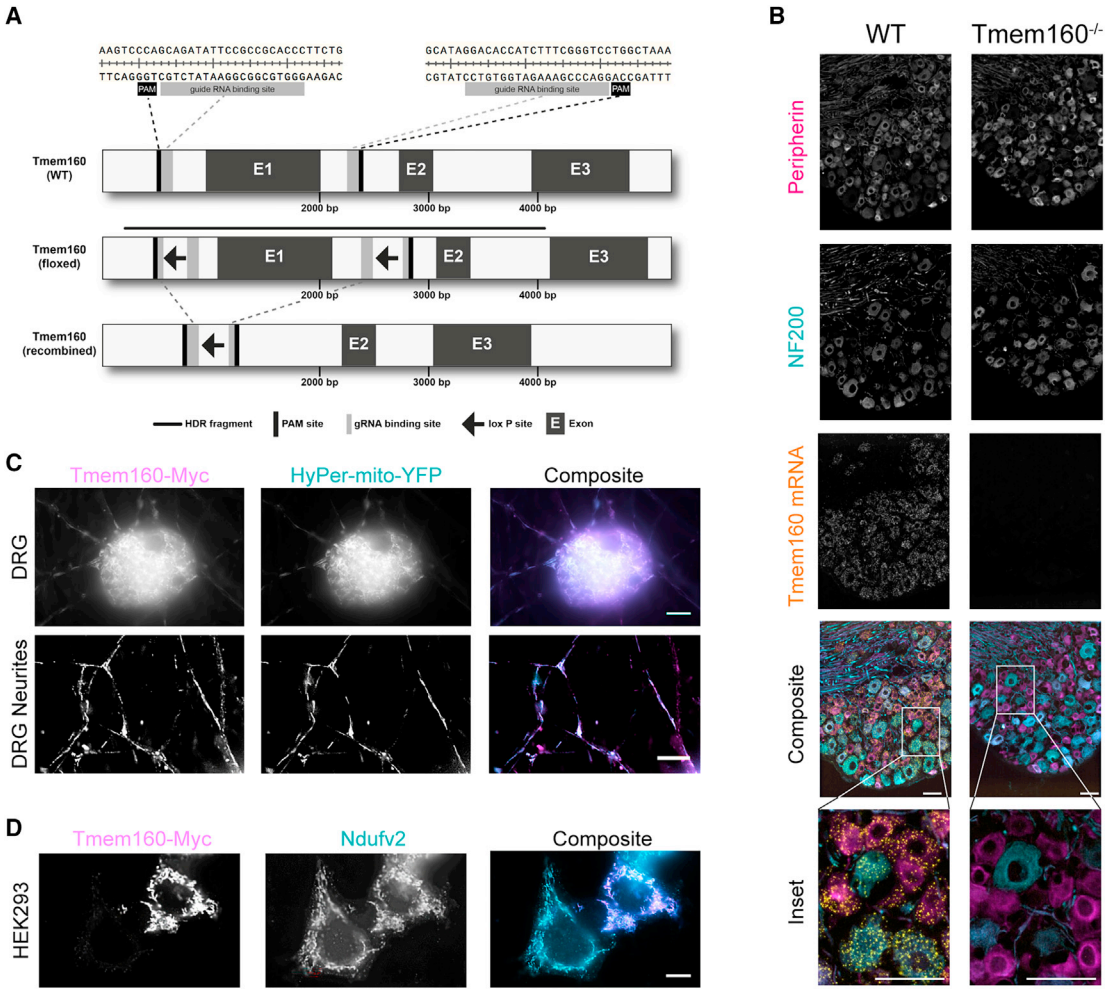

Figure 1. Tmem160 is expressed in mouse peripheral sensory neurons of DRG and is localized to mitochondria

(A) Generation of a global *Tmem160* knockout (KO; Tmem160$^{-/-}$) mouse line by CRISPR-Cas9 technology.

(B) Validation of Tmem160$^{-/-}$ in whole DRG using RNAscope technology followed by immunohistology with Peripherin and NF200. *Tmem160* mRNA is expressed in DRG sensory neurons of WT littermates independent of cell size and is absent in DRG of Tmem160$^{-/-}$ mice. Inset, magnification of indicated area. Scale bar, 50 μm. N = 3 mice/genotype.

(C and D) Confirmation of mitochondrial localization of the Tmem160 protein. Myc-tagged Tmem160 (Tmem160-Myc) co-localized with mitochondrial markers (HyPer-mito-YFP, Ndufv2) in somata and neurites of DRG cultures (C) and HEK293T cells (D). Scale bar, 10 μm. n = several coverslips from N = 4 independent DRG cultures (C) and N = 3 independent HEK293T cell cultures (D).

was altered in KO mice compared with WT mice (Figures 3B, 3C, S2A, and S2B). In addition, we investigated gait characteristics via the CatWalk XT gait analysis system (Noldus, NL) with a particular focus on select static (print area: area of the complete footprint; stand: duration of ground contact for a single paw; Figures S2A and S2B) and dynamic (swing phase: the time when the hindpaw was not in contact with the glass plate; duty cycle: duration of hindpaw contact divided by time between consecutive hindpaw contacts; Figures S2A and S2B) gait parameters. In analogy to clinically relevant movement-evoked pain in patients with pain, these parameters have been shown to be indicative of pain- and/or disability-induced changes in locomotion in rodent models of unilateral injuries (Pitzer et al., 2016; Cunha et al., 2020; Segelcke et al., 2021), e.g., "limping" or an antalgic (pain-avoiding) gait, defined by a reduced stand phase relative to the swing phase. KO and WT littermates did not differ in any measured gait parameter regardless of the pain entity (Incision or CFA; Figures S2A and S2B).

Next, we evaluated neuropathic pain induced by unilateral sciatic nerve injury (spared nerve injury model [SNI-model] [Decosterd and Woolf, 2000]; Figures 3D and S3). Again, NEP was similar among genotypes over the entire observation period up to 28 days after SNI, validating that nerve injury was successfully induced (Figures 3D and S3A). Strikingly, however, tactile hypersensitivity was largely absent in *Tmem160* KO mice 7 days after SNI (Figures 3D and S3B). In contrast, WT littermates showed marked tactile hypersensitivity at 7 days after SNI, as expected. At later time points (14–28 days after SNI), KO mice behaved similarly to WT littermates upon both SNI (Figures 3D and S3B) and sham surgery (Figure S3). Moreover, KO and WT littermates

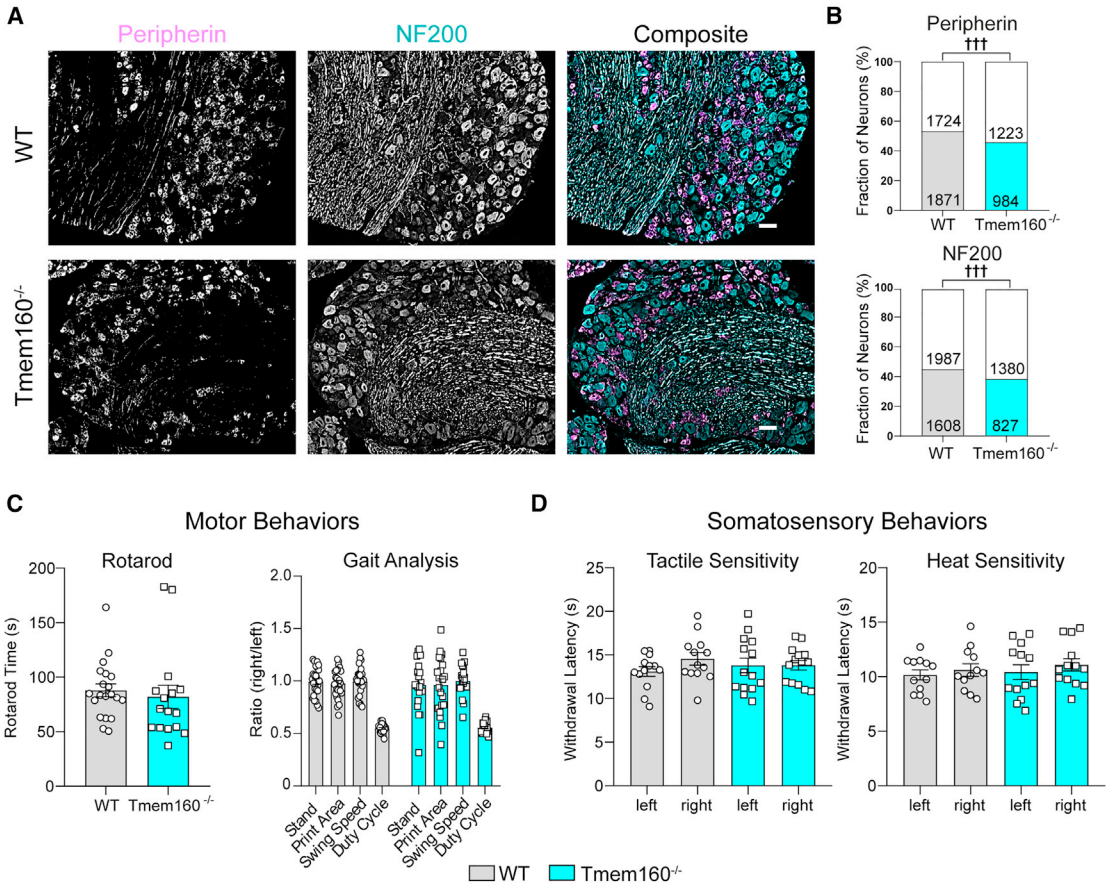

Figure 2. Tmem160 is dispensable for motor function and basal somatosensation

(A and B) Expression of Peripherin and NF200 as assessed by immunohistology in cryosections of DRG. Albeit significant overall given the high number of neurons quantified, observed differences in neuronal fractions are minimal between Tmem160$^{-/-}$ and WT mice. Fisher's exact test. † for comparison between genotypes. †††$p \leq 0.001$. Scale bar, 50 μm. Numbers indicate the number of neurons quantified (color/grey: positive label for respective marker; white: no label for respective marker). N = 5 (WT) and N = 3 (Tmem160$^{-/-}$) mice.

(C and D) Tmem160$^{-/-}$ mice displayed unaltered motor functions regarding coordination (Rotarod, time in seconds) and locomotion (gait analysis, ratio right/left hindpaw) compared with WT littermates (C) as well as WT-like somatosensory thresholds (D). Data are represented as mean ± SEM in a scatter bar plot. Two-way ANOVA followed by Holm-Sidak's multiple comparison tests, ns. (C) N = 20 (WT) and N = 16 (Tmem160$^{-/-}$) mice. (D) N = 13 (WT) and N = 14 (Tmem160$^{-/-}$) mice.

exhibited a pronounced antalgic gait after SNI (Figures S3C–S3F). It is noteworthy, thus, that gait parameters were slightly less (albeit not significantly) affected in KO mice when comparing post-SNI with pre-SNI values (Figures S3C–S3F). After sham surgery, the gait parameters were essentially similar among genotypes, confirming again the WT-like motor coordination in KO mice (Figures S3C–S3F). Taken together, our thorough behavioral analysis suggests that global *Tmem160* deficiency delays the establishment of tactile hypersensitivity explicitly during SNI-induced neuropathic pain. In contrast, the maintenance of neuropathic pain and other neuropathic pain-related behaviors as well as incision- and CFA-related pain behaviors appear to be largely independent of Tmem160.

Mitochondrial function appears to be unaffected by Tmem160 deficiency

Since Tmem160 localizes to mitochondria (Figures 1D and S1C), we hypothesized a role for Tmem160 in the context of mitochondrial (patho-) physiology, which might underlie the pain-related phenotype in KO mice. Mitochondrial dysfunction has emerged as a prominent player in pathological pain affecting cellular energy metabolism, calcium homeostasis, and oxidative stress (Bennett et al., 2014; Flatters, 2015; Yang et al., 2018; Li et al., 2020). Quantitative PCR suggested mildly reduced transcript levels of several electron transport chain (ETC) components in DRG of KO mice (Figure S4A). However, we did not find any apparent functional alterations in mitochondria of *Tmem160* KO mice compared with WT littermates when assessing (1) the complex IV activity in DRG lysates using a commercially available enzymatic activity assay (dipstick format) (Figure S4B), (2) the mitochondrial oxygen consumption rate (OCR) in brain lysates by established Seahorse assays (Duggett et al., 2016) (Figure S4C), and (3) the integrity of the mitochondrial membrane potential in cultured DRG after incubation with the mitochondrial dye tetramethylrodamine methyl ester (TMRM [Nicholls and Budd, 2000; Cannino et al., 2012]) (Figure S4D). Collectively

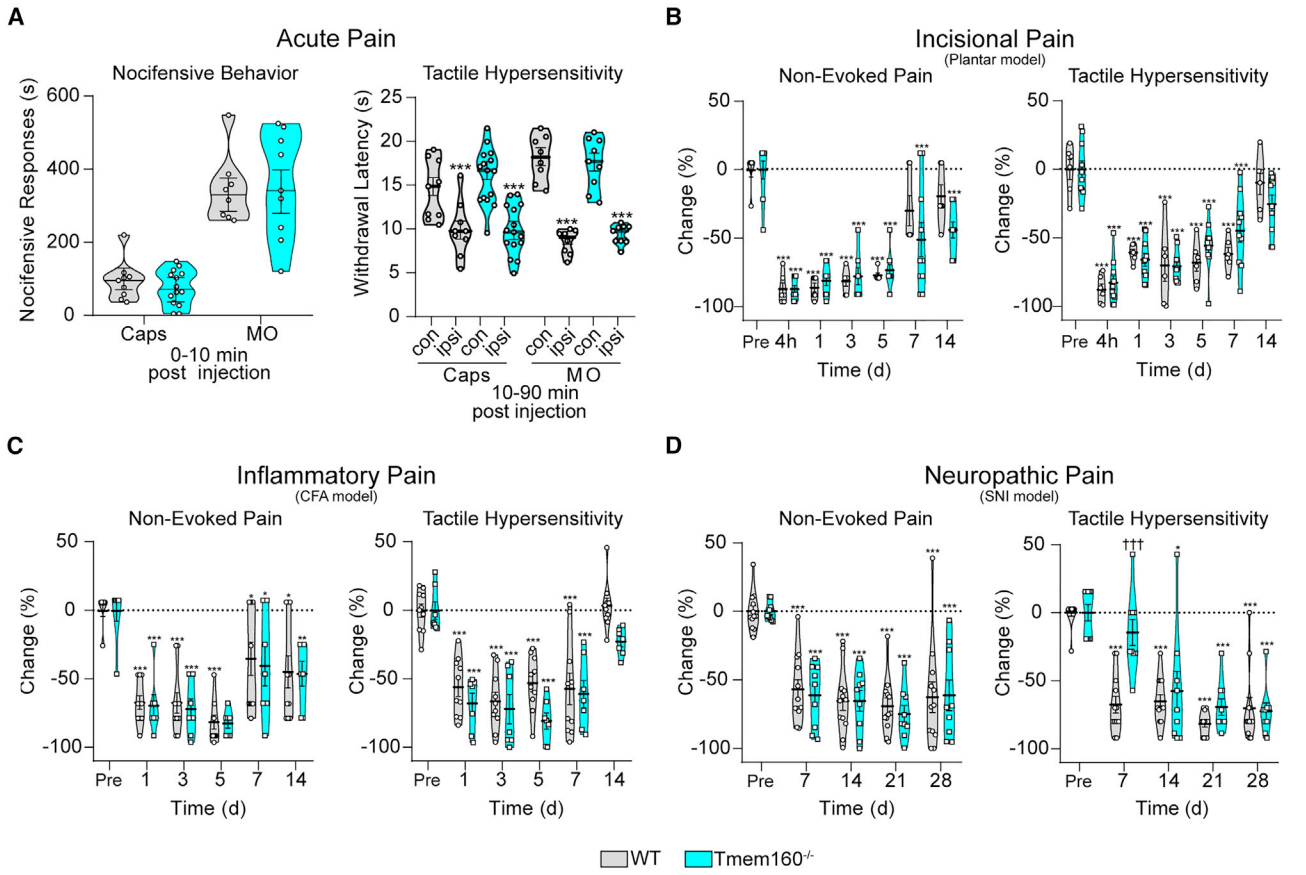

Figure 3. *Tmem160* deficiency specifically delays the establishment of tactile hypersensitivity during neuropathic pain in male mice

(A) Injection of Capsaicin (Caps) or mustard oil (MO) resulted in similar acute nocifensive responses (left) and tactile hypersensitivity (right) in the ipsilateral paw (ipsi) compared with the contralateral site (con) in WT littermates and Tmem160$^{-/-}$ mice. Caps: N = 9 (WT) and N = 15 (Tmem160$^{-/-}$) mice. MO: N = 8 (WT) and N = 9 (Tmem160$^{-/-}$) mice. Two-tailed unpaired t test for comparison between ipsi- and contralateral paws. ***p $\leq$ 0.001.

(B) Unilateral plantar incision (plantar model of incisional pain) induced similar non-evoked pain behavior and tactile hypersensitivity in WT littermates and Tmem160$^{-/-}$ mice over the entire observation period (up to 14 days). N = 6 (WT) and N = 10 (Tmem160$^{-/-}$) mice.

(C) Unilateral injection of complete Freund's adjuvant (CFA; model of inflammatory pain) into one hindpaw induced similar non-evoked pain behavior and tactile hypersensitivity in both genotypes over the entire observation period (up to 14 days). N = 10 (WT) and N = 7 (Tmem160$^{-/-}$) mice.

(D) Unilateral spared nerve injury (SNI) resulted in similar non-evoked pain in both genotypes over the entire observation period (up to 28 days). In Tmem160$^{-/-}$ mice, tactile hypersensitivity was significantly attenuated (††† $\leq$ 0.001) 7 days post SNI. N = 10 (WT) and N = 7 (Tmem160$^{-/-}$) mice.

(B–D) Data are displayed as change in percentage (mean ± SEM) relative to the mean pre-value in a scatter violin plot. To eliminate increasing body weight over the experimental period as a confounding factor, non-evoked pain behavior is expressed as the ratio between the treated (ipsilateral) and untreated (contralateral) hindpaw. Statistics was only performed on raw data (Figures S2 and S3). Two-way ANOVA followed by Holm-Sidak's multiple comparison tests. Asterisk (*) for comparison between ipsi- and contralateral paws. *p $\leq$ 0.05, **p $\leq$ 0.01, ***p $\leq$ 0.001. † for comparison between genotypes; ††† $\leq$ 0.001.

these data let us conclude that overall mitochondrial function is likely unaffected by *Tmem160* deficiency.

Tmem160 deficiency alters the inflammatory cytokine/chemokine profile in DRG

In the search for mechanistic molecular insights into the discrete phenotype of *Tmem160* KO mice (Figure 3D), we also considered neuroimmune and inflammatory signaling. In fact, neuroimmune interactions and inflammation have been shown to act as significant drivers of tactile hypersensitivity within the first week after nerve injury in the SNI model (Peng et al., 2016; Cobos et al., 2018). To test whether inflammatory signaling pathways were altered in *Tmem160* KO mice, we used a commercially available cytokine and chemokine array (Liu et al., 2019). This enabled us to simultaneously assess the relative protein abundance of 40 cytokines in lysates of DRG from naïve male KO mice and their WT littermates (Figures 4A and S5). Remarkably, we observed a pronounced downregulation of pro-and anti-inflammatory cytokines/chemokines in DRG of male KO mice. For example, many pro-inflammatory cytokines appeared reduced, such as interferon-gamma (IFNy), members of the CCL family (e.g., CCL4 and CCL12), several interleukins (ILs; e.g., IL1β, IL2, and IL23 and its downstream factors IL6 and IL17), and also tumor necrosis factor-alpha (TNFα) (Figure 4A). A straightforward interpretation of the net effect of this modulation of inflammatory signaling is difficult, given its complexity (Ji et al., 2016). Nonetheless, these results may hint at a shift of the cytokine/chemokine profile of male KO DRG towards an anti-inflammatory state.

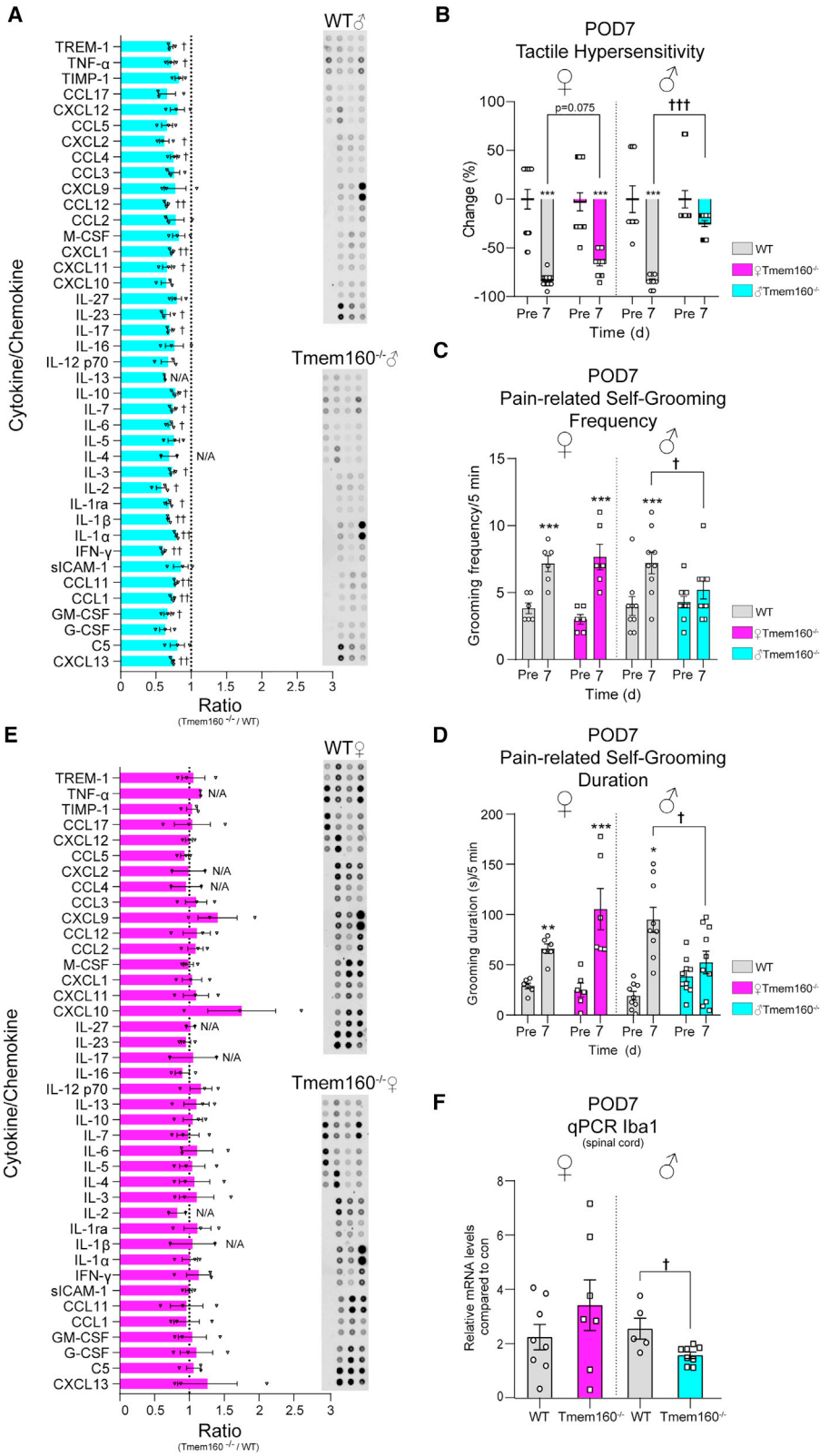

(legend on next page)

Sexually dimorphic role of Tmem160 for the establishment of discrete nerve injury-induced pain behaviors

In the context of neuroimmune interactions, prominent sexual dimorphism has been reported (Mogil, 2012; Sorge et al., 2015; Mapplebeck et al., 2016; Lopes et al., 2017b; Rosen et al., 2017). Having shown modified cytokine/chemokine profiles in naïve male KO mice (Figure 4A) and delayed tactile hypersensitivity upon SNI (Figure 3D), we next turned to test pain-related behaviors in female KO mice (Figures 4B–4D and S6A–S6F). Strikingly, SNI-induced tactile hypersensitivity in female KO mice was similar to female WT littermates 7 days post SNI (Figures 4B and S6B), in stark contrast to our observations in male KO mice (Figures 4B and 3D). Note, however, that despite pronounced tactile hypersensitivity, female KO mice showed a tendency ($p = 0.075$) toward smaller changes in tactile thresholds compared with female WT littermates (Figure 4B). NEP behavior and locomotion characteristics did not differ among genotypes in females (Figures S6A and S6C–S6F), analogous to our data in male KO mice (Figures 3D, S3A, and S3C–S3F). To extend our behavioral analysis, we additionally investigated the impact of SNI on changes in self-grooming as an example of rodent-specific behaviors (Cunha et al., 2020). Interestingly, the aforementioned sexual dimorphism was also reflected in alterations of pain-related self-grooming. Its frequency and duration (Figures 4C and 4D) were markedly attenuated in male but not female KO mice 7 days post SNI. Taken together, these data suggest that the attenuation of tactile hypersensitivity and changes in pain-related self-grooming is sexually dimorphic in *Tmem160* KO mice and largely specific to males 7 days post SNI.

Correlating with our findings on pain-related behaviors, naïve female KO mice displayed a WT-like DRG cytokine/chemokine profile (Figure 4E) in contrast with male KO mice (Figure 4A). Moreover, we performed quantitative PCR for *Iba1*, a widely used marker for microglia activation, to explore the central immune response in the spinal cord 7 days post SNI. As expected, *Iba1* transcript levels were strongly upregulated in the ipsilateral spinal cords of male and female WT mice (as compared with the contralateral side) but significantly less so in male KO mice (Figure 4F). This difference in spinal Iba1-levels between KO and WT males was not apparent 28 days post SNI (Figure S6G), in line with WT-like tactile hypersensitivity in KO males as shown above (Figures 3D and S3B). In summary, the results from female KO mice (Figures 4E and 4F) contrast the dampened cytokine/chemokine profile (Figure 4A) and attenuated Iba1 regulation observed in male KO mice (Figure 4F), lending strong support to a sexually dimorphic role of Tmem160 for neuroimmune signaling specifically in the early phase after SNI.

These findings prompt the question whether Tmem160 exerts its function in DRG sensory neurons, immune cells, or both. Recent efforts in RNA-seq profiling of spinal microglia in the SNI model discovered *Tmem160* to be specifically expressed in a small microglia population (referred to as cluster 9 microglia) with a marked inflammatory profile (Tansley et al., 2020). Even more, it could be shown that cluster 9 microglia were absent in naïve mice (0.035% of total microglia) but were substantially increased (4.9% of total) only in the early phase of neuropathic pain (3 days post SNI) and exclusively in male but not female mice (Tansley et al., 2020)—bearing a strong resemblance to the observations we report here in global KO *Tmem160* mice. While we cannot assess the functional role of cluster 9 microglia experimentally due to their aforementioned scarcity, we generated conditional KO (cKO) mice (Advillin Tmem160$^{-/-}$) using the Advillin-Cre driver line to delete *Tmem160* in the majority (approximately [approx.] 80% [Zurborg et al., 2011]) of DRG sensory neurons. The successful conditional deletion of *Tmem160* was confirmed by genotyping (please see STAR Methods for details) and quantitative PCR in DRG (remaining *Tmem160* transcript level = 11% ± 1% of floxed littermate controls, Tmem160$^{fl/fl}$; N = 8 mice/genotype). Remarkably, and in contrast to global KO males, we did not observe any alterations in the

Figure 4. *Tmem160* deficiency alters the DRG cytokine/chemokine profile and neuropathy-related pain behaviors in a sexually dimorphic manner

(A) Pronounced downregulation of diverse pro- and anti-inflammatory cytokines and chemokines in naïve Tmem160$^{-/-}$ mice compared with WT littermates. Exemplary images of the membranes for WT (top) and Tmem160$^{-/-}$ male mice (bottom). Data are depicted as mean ± SEM in a scatter bar plot displaying the ratio of the abundance of each cytokine/chemokine between male KO and WT mice, ratio KO/WT. Ratio-paired t tests. † for comparison between genotypes. †$p \leq 0.05$, ††$p \leq 0.01$. If ≤2 values/genotype were obtained per cytokine/chemokine, the significance could not be assessed (N/A). N = 6 (WT) and N = 6 (Tmem160$^{-/-}$) mice. n = 3 membranes/genotype.

(B–D) Seven days after SNI, Tmem160$^{-/-}$ males (independent cohort from data in Figure 3D), but not females, exhibited attenuated tactile hypersensitivity (B) as well as significantly reduced pain-related self-grooming (C and D). Tactile hypersensitivity is displayed as the percentage change relative to the mean pre-value in a scatter bar plot (B). Pain-evoked self-grooming is expressed by frequency (C) and duration in seconds (D) over a 5 min observation period analyzed by two independent experimenters (please see STAR Methods for details, inter-rater reliability [degree of agreement among independent raters], $\kappa = 0.852$ for frequency and $\kappa = 0.785$ for the duration, κ was interpreted according to guidelines from Cicchetti and Sparrow [Cicchetti and Sparrow, 1981]: 0.0 = poor to 1.0 = excellent). Self-grooming data are displayed as mean ± SEM in a scatter bar plot (C and D). (B–D) Two-way ANOVA followed by Holm-Sidak's multiple comparison tests on raw data. Asterisk (*) for comparison relative to pre-values/sex. † for comparison between genotypes/sex. */†$p \leq 0.05$, **$p \leq 0.01$, ***/†††$p \leq 0.001$. (B) Females: N = 14 (WT) and N = 16 (Tmem160$^{-/-}$) mice. Males: N = 9 (WT) and N = 15 (Tmem160$^{-/-}$). (C and D) Females: N = 6 (WT) and N = 6 (Tmem160$^{-/-}$) mice. Males: N = 9 (WT) and N = 15 (Tmem160$^{-/-}$).

(E) DRG from naïve female Tmem160$^{-/-}$ mice displayed a WT-like cytokine/chemokine profile. Exemplary images of the membranes for female WT littermates (top) and Tmem160$^{-/-}$ (bottom) mice. Data are depicted as mean ± SEM in a scatter bar plot displaying the ratio of the abundance of each cytokine/chemokine between female KO and WT mice, ratio KO/WT. Ratio-paired t tests, ns. If ≤2 values/genotype were obtained per cytokine/chemokine, the significance could not be assessed (N/A). N = 6 (WT) and N = 6 (Tmem160$^{-/-}$) mice. n = 3 membranes/genotype.

(F) At 7 days post SNI, Iba1 mRNA levels were upregulated in the ipsilateral spinal cord (compared with the contralateral side) in female WT and Tmem160$^{-/-}$ mice as well as in male WT mice, but were significantly less so in KO males. Data are depicted as mean ± SEM in a scatter bar plot. Mann-Whitney test between genotypes within sex, † ≤ 0.05. Females: N = 8 (WT) and N = 7 (Tmem160$^{-/-}$) mice. Males: N = 5 (WT) and N = 8 (Tmem160$^{-/-}$) mice.

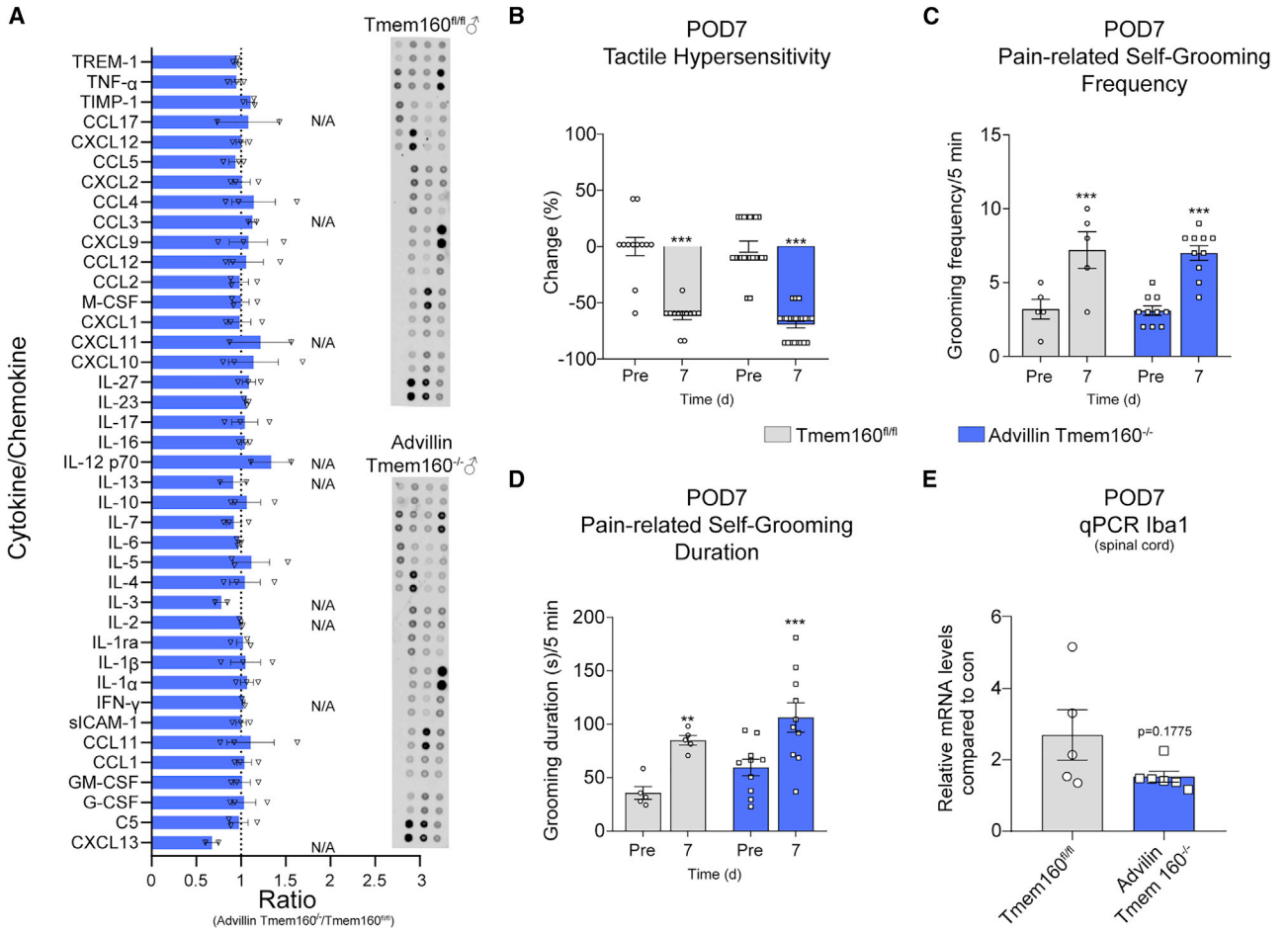

Figure 5. Tmem160 deficiency in Advillin-positive sensory neurons neither alters the DRG cytokine profile nor neuropathy-induced behaviors or *Iba1* levels in male mice

(A) No apparent changes of cytokines/chemokines in DRG of naïve Advillin-Cre Tmem160$^{-/-}$ (cKO; Advillin Tmem160$^{-/-}$) males compared with floxed male littermate controls (Tmem160$^{fl/fl}$). Exemplary images of the membranes for Tmem160$^{fl/fl}$ (top) and Advillin Tmem160$^{-/-}$ males (bottom). Data are represented as mean ± SEM in a scatter bar plot. Ratio-paired t tests, ns. If ≤ 2 values/genotype were obtained per cytokine/chemokine, the significance could not be assessed (N/A). N = 6 (WT) and N = 6 (cKO) mice. n = 3 membranes/genotype.

(B–D) Pronounced tactile hypersensitivity and pain-related self-grooming in both floxed male littermate controls (Tmem160$^{fl/fl}$) and cKO (Advillin Tmem160$^{-/-}$) 7 days post SNI. Tactile hypersensitivity is displayed as the percentage change (and SEM) relative to the mean pre-value in a scatter bar plot (B). Pain-evoked self-grooming is expressed by frequency (C) and duration in seconds (D) over a 5 min observation period analyzed by two independent experimenters (please see STAR Methods for details, inter-rater reliability [degree of agreement among independent raters], κ = 0.882 for frequency and κ = 0.815 for duration, κ was interpreted according to guidelines from Cicchetti and Sparrow [Cicchetti and Sparrow, 1981]: 0.0 = poor to 1.0 = excellent). Self-grooming data are displayed as mean ± SEM in a scatter bar plot (C and D). Two-way ANOVA followed by Holm-Sidak's multiple comparison tests on raw data. Asterisk (*) for comparison relative to pre-values. *p ≤ 0.05, **p ≤ 0.01, ***p ≤ 0.001. (C and D) N = 5 (Tmem160$^{fl/fl}$, grey) and N = 10 (Advillin Tmem160$^{-/-}$, blue).

(E) 7 days post SNI, *Iba1* mRNA levels were upregulated in the ipsilateral spinal cord (compared with the contralateral side) in both floxed male littermate controls (Tmem160$^{fl/fl}$) and cKO (Advillin Tmem160$^{-/-}$) males. Data are depicted as mean ± SEM in a scatter bar plot. Mann-Whitney test between genotypes, p = 0.1775. N = 5 (Tmem160$^{fl/fl}$, grey) and N = 6 (Advillin Tmem160$^{-/-}$, blue).

DRG cytokine/chemokine profile of cKO males (Figure 5A). 7 days post SNI, pain-related behaviors (Figures 5B–5D, S6H, and S6I) were largely similar to floxed male littermate controls (Tmem160$^{fl/fl}$), in which Advillin-Cre was not expressed. Correlating with the behavioral data 7 days post SNI, *Iba1* transcripts were increased in both genotypes in the ipsilateral spinal cord, albeit slightly less so (p = 0.1775, not significant [ns]) in cKO males compared with floxed controls (Figure 5E). These results point toward a role of Tmem160 in non-neuronal cells, possibly including immune cells and the recently discovered cluster 9 microglia population in males (Tansley et al., 2020). Note, however, that Advillin-Cre-mediated recombination is reported to spare approx. 20% of DRG sensory neurons (Zurborg et al., 2011); therefore, we cannot exclude an involvement of Tmem160 expressed in DRG sensory neurons.

What could be the functional consequences and molecular targets of alterations in the cytokine/chemokine profile in DRG of male global KO mice? Previous work has demonstrated

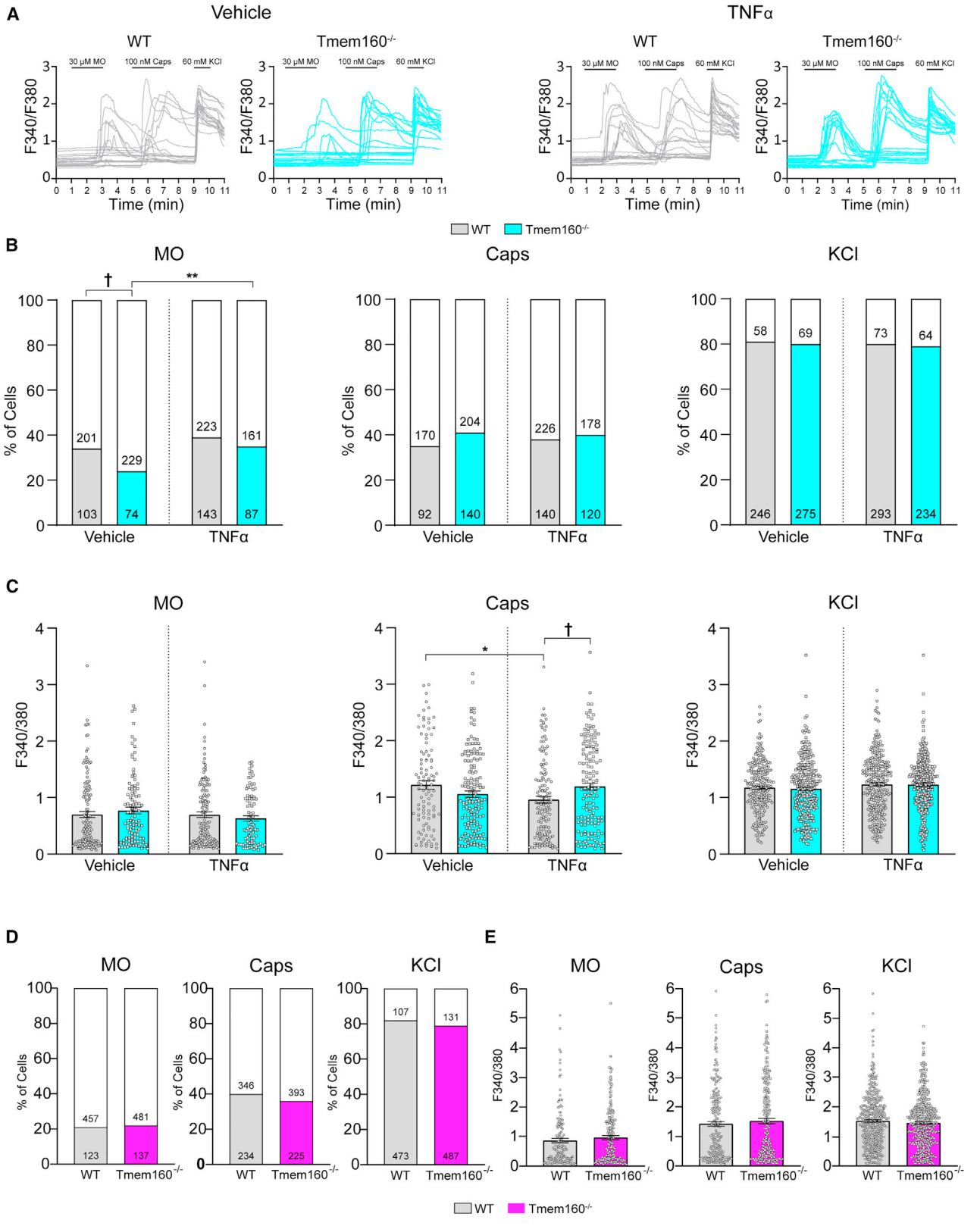

(legend on next page)

that, among others, transient receptor potential (TRP) channels, in particular TRPA1 and TRPV1, are regulated by cytokines (Guan et al., 2016). For example, TNFα was shown to modulate TRPA1 and TRPV1 membrane trafficking and activity (Meng et al., 2016). To investigate whether *Tmem160* deficiency and the associated reduction of TNFα affected TRPA1- or TRPV1-mediated neuronal activity, we performed calcium imaging in DRG cultures from naïve, untreated mice (Figure 6). In this way, we monitored TRPA1-induced (in response to 30 μM MO) and TRPV1-induced (in response to 100 nM Caps) neuronal responses, as well as overall neuronal activity (in response to 60 mM KCl). We further compared control conditions (pre-incubation with the vehicle) with the exogenous application of TNFα (100 ng, 6 h, as published elsewhere [Hanack et al., 2015; Willemen et al., 2018]) (Figure 6A–6C). The latter experiment was designed to compensate for the aforementioned endogenous TNFα reduction in DRG from KO males (Figure 4A). Under control conditions, *Tmem160*-deficient male DRG cultures exhibited WT-like MO response amplitudes (Figures 6A and 6C) but reduced cellular response profiles to MO, as quantified by comparing the percentage of responding neurons among genotypes (Figures 6A and 6B). Intriguingly, the exogenous application of TNFα was able to rescue this defect in MO-responsiveness in KO cultures (Figures 6A and 6B). In contrast, TRPV1-mediated and KCl-induced activity were mostly similar among genotypes (Figures 6A–6C) except for slightly larger Caps-response amplitudes in KO DRG upon the application of TNFα (Figure 6C). These results suggest that, in male mice, Tmem160 may act mechanistically by modulating TRPA1-mediated neuronal activity in concert with TNFα and possibly other yet-to-be-identified factors. As TRPV1-mediated neuronal activity is prone to desensitization, we separately performed calcium imaging using two different Caps concentrations without the prior addition of MO (Figure S7A and S7B). No overt differences in TRPV1-mediated response amplitudes or cellular response profiles could be discerned between KO and WT cultures. We then performed calcium imaging in DRG cultures derived from female mice, which showed activity similar to female WT littermates (Figures 6D and 6E). Also, we did not observe significant alterations of neuronal responses in cKO males, in which Tmem160 was deleted in the majority of DRG sensory neurons by Advillin-Cre-induced recombination, compared with floxed male littermates (Figures S7C and S7D). In summary, this data lends further support to a male-specific role of Tmem160 for mediating neuroimmune interactions likely in non-neuronal cells.

DISCUSSION

In order to obtain deeper mechanistic insights into pain entities, the identification of candidates specifically implicated in pathological but not acute pain is of high priority. Here, we characterized Tmem160 and demonstrated its significance in a pain-entity-specific, modality-specific, and sexually dimorphic manner: in male mice, Tmem160 is explicitly implicated in establishing tactile hypersensitivity and pain-related changes of self-grooming upon SNI-induced neuropathic pain. Mechanistically, we show that only male *Tmem160* KO mice exhibit dampened neuroimmune signaling, as suggested by a reduction of (1) cytokine and chemokine levels in DRG, (2) microglia in the spinal cord 7 days post SNI, and (3) TRPA1-mediated neuronal activity regulated by TNFα. These findings are of high relevance, as our study reveals Tmem160 to be implicated in specific neuropathic-pain-related behaviors and neuroimmune signaling in male mice.

We used an extensive set of pain models and behavioral paradigms to comprehensively assess motor, sensory, and pain-related modalities in *Tmem160* KO mice. Considering the debate on the translational potential of behavioral assessments in rodents (Mogil, 2009; Gereau et al., 2014; Mogil, 2020), we included classical reflexive-based assays (withdrawal to tactile and heat stimulation), a functional investigation of gait alterations representing aspects of movement-evoked pain, measures of NEP (Segelcke et al., 2021), and pain-related alterations of rodent-specific behaviors (Turner et al., 2019; Mogil, 2020) such as self-grooming (Callahan et al., 2008). The latter is indicated in preclinical research to avoid anthropomorphizing obtained results from rodents (Vasconcelos et al., 2012; Du Percie Sert and Rice, 2014). Moreover, we harnessed the advantages of a video-based assessment of mouse behaviors (i.e., NEP, locomotion, and self-grooming in this study) to limit the experimenter's influence on outcome measures (Sorge et al., 2014; Mogil, 2020). In this way, we were able to unravel a distinct phenotype in *Tmem160* global KO males: the delayed establishment of tactile hypersensitivity and attenuated pain-related self-grooming, specifically in the early phase of neuropathic pain. We did not observe alterations in other modalities commonly affected by nerve injury-induced neuropathic pain such as NEP and locomotion. Changes in pain-related self-grooming might serve a

Figure 6. Tmem160 modulates TRPA1-mediated neuronal activity specifically in males

(A–C) Ratiometric Ca^{2+} imaging was performed in cultured DRG neurons of naïve Tmem160$^{-/-}$ and WT males. After incubation with exogenous TNFα (100 ng) or vehicle (PBS) for 6 h, stimuli were applied from minute 1 to 3 (MO, 30 μM), 5 to 7 (Caps, 100 nM), and 9 to 10 (KCl, 60 mM); please see black bars in (A). (A) Representative traces and stimulation protocol. (B) Percentage of responding (colored part) and non-responding (white part) neurons to indicated stimuli. Numbers represent the total number of neurons imaged. DRG cultures from Tmem160$^{-/-}$ males exhibited significantly less responders to MO, which could be rescued to a WT-level upon exogenous application of TNFα. (C) Scatter bar plots represent the maximal amplitudes (mean ± SEM) of responding neurons to indicated stimuli. Genotypes were largely similar except for a mild increase of Caps-response amplitudes in Tmem160$^{-/-}$ DRG compared with WT DRG upon application of TNFα.

(D–E) Ratiometric Ca^{2+} imaging was performed in cultured DRG neurons of naïve Tmem160$^{-/-}$ and WT females exactly as described above for males yet without incubation with TNFα. No differences among genotypes could be discerned. (D) Percentage of responding (colored part) and non-responding (white part) neurons to indicated stimuli. Numbers represent the total number of neurons imaged. (E) Scatter bar plots represent the maximal amplitudes (mean ± SEM) of responding neurons to indicated stimuli.

(B and D) Fisher's exact test. (C and E) Mann-Whitney Test. All tests: asterisk (*) for comparison to vehicle control. † for comparison between genotypes. */†$p \leq 0.05$, **$p \leq 0.01$. For both genotypes and sexes, multiple coverslips from N = 3 mice were used.

distracting role (Callahan et al., 2008) and promote well-being and potentially hypoalgesia (Callahan et al., 2008). While only speculative at this point, self-grooming might cause hypoalgesia via spinal inhibitory interneurons under the control of grooming-activated skin A-fibers (Beyer et al., 1985). In contrast, KO mice displayed normal motor function and sensory thresholds and WT-like nociceptive acute incisional and inflammation-induced (via CFA injection) pain-related behaviors. Notably, the phenotype observed in *Tmem160* global KO mice appears to be specific to males as female KO mice exhibited WT-like behaviors in all tested paradigms. Thus, the extensive behavior characterization carried out in this study enabled us to reveal a male-specific role of Tmem160 in the establishment of neuropathy-associated tactile hypersensitivity and—either directly or as a consequence—in pain-related changes in self-grooming.

Tmem160 is broadly expressed in peripheral sensory neurons of mouse DRG. Furthermore, transcriptome-based datasets (Thakur et al., 2014; Usoskin et al., 2015) (database: mousebrain.org [Zeisel et al., 2018]) show experimental evidence for *Tmem160* expression across a wide range of tissues/cell types, including immune cells such as the recently discovered low abundant cluster 9 of microglia in male mice (Tansley et al., 2020). Nevertheless, we did not observe any significant fertility, motor, or somatosensory alterations in *Tmem160* KO mice. Our immunohistochemistry experiments demonstrate that global *Tmem160* deletion neither causes overt morphological changes nor prominent neuronal loss in DRG. Overall, the specific delay in establishing tactile hypersensitivity is unlikely to be caused by developmental defects in DRG of *Tmem160* KO mice or generalized dysfunction in transmitting sensory, especially nociceptive, information.

How does Tmem160 contribute to tactile hypersensitivity during neuropathic pain? We tested several hypotheses: (1) mitochondrial dysfunction, (2) altered neuroimmune signaling, and, consequently, (3) changes in neuronal activity. Since (i) Tmem160 is predicted to be integrated into mitochondrial membranes and harbors a mitochondrial import sequence, (ii) our immunolabeling and biochemical experiments validated ubiquitous mitochondrial co-localization, and (iii) mitochondria, or rather their dysfunction, are critically involved in neuropathic pain (Bennett et al., 2014; Flatters, 2015; Yang et al., 2018; Li et al., 2020), we performed a comprehensive set of experiments to assess the functional integrity of mitochondria in KO mice. However, we could not find any indication supporting a functional role of Tmem160 in the context of mitochondria. On the other hand, we cannot entirely rule out mild mitochondrial ETC defects in discrete neuronal or immune cell subpopulations of *Tmem160*-deficient DRG, which likely might have escaped our global—yet well established and commonly used (Dennerlein et al., 2015; Aich et al., 2018)—analysis methods. Even so, our data collectively suggest that ETC-dependent mitochondrial signaling likely plays a minor mechanistic role for the observed phenotype, if at all.

Global *Tmem160* KO mice did not develop tactile hypersensitivity during the first week following nerve injury but did thereafter (14 and 28 days post SNI). Intriguingly, this time course bears a resemblance to previous reports on the importance of neuroimmune signaling in DRG (Cobos et al., 2018). In particular, peripheral monocytes and microglia (Vicuña et al., 2015; Peng et al., 2016) appear to be implicated in early tactile hypersensitivity but not for its maintenance under neuropathic pain conditions. Our study carefully compared cytokine and chemokine levels—representing soluble effectors of immune signaling—between KO and WT mice and observed a globally dampened profile in KO males but not females. Importantly, not only pro-inflammatory mediators (e.g., IL1β, IL6, and TNFα) were affected in *Tmem160* KO males but also anti-inflammatory ones such as IL2 and IL10. This observed complexity is in keeping with previous reports, which highlighted the significance of balancing pro- and anti-inflammatory mediators for the outcome of neuropathic pain (Lees et al., 2013; Grace et al., 2014; Kiguchi et al., 2015; Niehaus et al., 2021). The mechanisms that prevent cytokine/chemokine production or release in Tmem160 KO males are unknown and require further study. Yet, we could show that the delay of SNI-mediated tactile hypersensitivity in KO males correlates with reduced microglia marker Iba1 levels in the spinal cord. Also, neuronal responses seem to be intact, as the exogenous application of the cytokine TNFα normalized TRPA1-mediated responses in KO DRG cultures. In addition, sensory neuron-specific cKO male mice, in which Tmem160 was deleted in 80% of DRG neurons, neither showed alterations in SNI-mediated tactile hypersensitivity nor were cytokine/chemokine and Iba1 levels or neuronal responses affected. These experiments suggest a significant (yet possibly not exclusive) role of Tmem160 in non-neuronal cells, which we hypothesize to be immune cells. In this context, the recent discovery of a very scarce microglia population, i.e., cluster 9 microglia, is of high relevance (Tansley et al., 2020). Among identified microglia clusters, cluster 9 exhibits a marked expression of *Tmem160* and a pronounced inflammatory profile. Furthermore, cluster 9 microglia are upregulated from 0.035% (of total microglia) to 4.9% (of total microglia) in the spinal cord of male but not female mice, specifically 3 days post SNI but not later (Tansley et al., 2020). This finding bears resemblance to the here-reported male-specific implication of Tmem160 for pain-related behaviors and neuroimmune signaling, specifically in the early phase of neuropathic pain. Therefore, we hypothesize that Tmem160-deficiency in cluster 9 microglia might contribute to the phenotype of attenuated SNI-associated tactile hypersensitivity in global KO male mice.

Future experiments are required to isolate this very small population of microglia 3 days post-SNI and assess the function of Tmem160 specifically in these cells. Besides cluster 9 microglia in the spinal cord, Tmem160 may play a role in subclasses of spinal (Niehaus et al., 2021) or peripheral (Yu et al., 2020) macrophages, both implicated in neuropathic pain. For the latter, single-cell profiling of DRG immune cell types at different time points post-SNI would be warranted to answer these open questions. Single-cell profiling of spinal cell types has just recently discovered a class of anti-inflammatory MRC1+ macrophages (Macro1 and Macro2) (Niehaus et al., 2021), which appear to restrain nerve injury-induced inflammation and pain. MRC1+ macrophages were also present in DRG. Interestingly, among all cell types (neuronal, immune, vascular, glial) analyzed upon SNI, *Tmem160* transcripts appeared to be downregulated in

one distinct excitatory neuron population (Excit15) and in the Macro2 subtype of MRC1+ macrophages, further substantiating our working hypothesis about its role in neuroimmune signaling.

Pro-inflammatory cytokines released by immune cells can drive sensitization of nociceptors and neuronal excitability by diverse mechanisms (Ji et al., 2016). For example, TNFα has been suggested to trigger pain-related behaviors through parallel downstream pathways comprising IL1β, CXCL1, or GM-CSF (Vicuña et al. 2015); in fact, we found all of these cytokines to be reduced in naïve *Tmem160* KO mice compared with WT littermates. In addition, the application of TNFα to DRG cultures was reported to increase membrane trafficking of TRP channels, such as TRPV1 and TRPA1, and thereby augmented responses to their respective agonists (Meng et al., 2016; Zhao et al., 2019). Consistent with these data, we observed that responsivity upon TRPA1-activation was diminished in cultured neurons of *Tmem160* global KO male mice but could be restored by the addition of TNFα, possibly compensating for lower endogenous TNFα levels in male KO DRG. We further show that the overall neuronal excitability and TRPV1-mediated responses were largely unaltered in KO DRG neurons, suggesting a certain degree of specificity for TRPA1 in peripheral sensory neurons. Nonetheless, *Tmem160* deficiency may likely affect additional receptors and signaling pathways given the known complexity of DRG neuron sensitization and mechanisms underlying neuropathy-induced pain behaviors (Costigan et al., 2009; Paldy et al., 2017; Wetzel et al., 2017).

It is worth mentioning, thus, that data generated in cultured DRG are not sufficient to discern a potentially neuronal requirement of Tmem160 from its function in non-neuronal cells such as satellite glia, fibroblasts, and macrophages—all of which were reported to be present in DRG cultures (Krames, 2014; Thakur et al., 2014; Ji et al., 2016; Cook et al., 2018; Price and Gold, 2018). It should also be noted that DRG isolation and culturing involves nerve injury, i.e., cutting the peripheral and central axons. Indeed, dissociated DRG cultures display transcriptional signatures that are suggestive of a neuropathic phenotype (Ono et al., 2012; Lopes et al., 2017a; Wangzhou et al., 2020), as inferred from the expression of inflammatory and immune markers. Thus, they represent a highly valuable *in vitro* system for mechanistic studies of neuropathic pain. In consequence, one needs to consider the possibility that the here-reported attenuation of TRPA1-mediated responses and cytokine/chemokine levels in male global KO DRG might rather be indicative of processes underlying neuropathy-related rather than physiological responses. Indeed, we do not see a behavioral correlate of dampened TRPA1-mediated neuronal activity in naïve mice, i.e., in mice without nerve injury: acute nociception to injection of the TRPA1-agonist MO was unaltered in KO male mice.

What about the role of Tmem160 in female mice? Here, we show that, in female mice, *Tmem160* appears to be dispensable for establishing tactile hypersensitivity and pain-related changes in self-grooming 7 days post SNI. Evidence is accumulating that mechanisms underlying pathological pain differ across sexes in mice and humans (Mogil, 2012; Sorge et al., 2015; Mapplebeck et al., 2016; Lopes et al., 2017b; Rosen et al., 2017): Microglia and peripheral macrophages play a prominent role in male mice (Sorge et al., 2011; Sorge et al., 2015; Lopes et al., 2017a; Yu et al., 2020), while the adaptive immune response via T cells seems to be more dominant in female mice (Sorge et al., 2015; Mapplebeck et al., 2016; Laumet et al., 2019). Even more complex, Peng and colleagues (Peng et al., 2016) described sexual dimorphism in tactile hypersensitivity only in the maintenance but not the initiation phase after nerve injury (in a spinal nerve transection model), whereas heat hypersensitivity was sex-independent. Moreover, they showed that the depletion of spinal cord microglia only delayed but did not reverse tactile hypersensitivity during neuropathic pain (Peng et al., 2016), similar to the phenotype of *Tmem160* KO mice described here.

For Tmem160, the exact molecular underpinnings and involved cell types contributing to its here-shown male-specific function in the early phase of neuropathic pain represents an exciting area of future inquiry. Even though the concrete function of peripheral and potentially central Tmem160 in pathological pain remains to be elucidated, the data presented here allow us to propose an attractive working model in male mice: during the early phase (up to 7 days) after SNI, Tmem160 may facilitate cytokine/chemokine release in DRG and the spinal cord either directly by immune cells or via bi-directional cross-talk between neurons and immune cells (Ji et al., 2016; Cook et al., 2018). In turn, augmented cytokine release is known to sensitize DRG neurons, thereby contributing to SNI-induced pain-related behaviors (Ji et al., 2016; Price et al., 2018). Accordingly, here we provide mechanistic evidence for Tmem160 to affect the (1) cytokine and chemokine levels in DRG, (2) TRPA1-mediated activity of DRG neurons synergistically with TNFα, and (3) microglia in the spinal cord specifically 7 days post SNI. Taken together, our results uncover Tmem160 as a male-specific player for distinct behavioral modalities and neuroimmune signaling in the setting of neuropathic pain.

Limitations of the study

In this study, we used global Tmem160 KO mice and cKO (conditional KO in peripheral sensory neurons) mice to characterize the functional role of Tmem160 for pain-related behaviors and neuroimmune signaling in DRG. Based on our results and very recent RNA-seq profiling of macrophages (Niehaus et al., 2021) and microglia (Tansley et al., 2020), we hypothesize a prominent role of Tmem160 in non-neuronal cell types such as microglia and/or macrophages. However, our data do not provide direct evidence for this working hypothesis. Thus, future experiments are required for further clarification of the cell types, in which Tmem160 exerts its function. These experiments need to involve genetic manipulation of Tmem160 expression in discrete populations of microglia and macrophages as well as other cell types of mouse DRG and the spinal cord. Similarly, given the known complexity of mechanisms underlying neuropathy-induced pain, Tmem160 may affect diverse receptors and signaling pathways in addition to the here-reported modulation of TRPA1 in DRG.

STAR★METHODS

Detailed methods are provided in the online version of this paper and include the following:

SUPPLEMENTAL INFORMATION

Supplemental information can be found online at https://doi.org/10.1016/j.celrep.2021.110152.

ACKNOWLEDGMENTS

The authors would like to thank Tanja Nilsson (MPI for Experimental Medicine, Goettingen, Germany) and Mirjam Augustin (Clinic for Anaesthesiology, Intensive Care Medicine and Pain Therapy, University Hospital Muenster, Germany) for excellent technical assistance; Dr. Luca Avenali (formerly MPI for Experimental Medicine, Goettingen, Germany) for preliminary experiments; Dr. Julia Sondermann (University of Vienna, Austria) and Dr. Sarah Flatters (formerly King's College London, UK) for helpful experimental advice; Dr. Ursula Fünfschilling and the transgenic facility at the MPI for Experimental Medicine for generating KO mice; the team of the AGCT-Lab at the MPI for Experimental Medicine for genotyping; Dr. med. vet. Sarah Kimmina (MPI for Experimental Medicine) for her help and support with animal welfare; and the team of animal caretakers at the animal house of the MPI for Experimental Medicine for their excellent work. We are grateful to all past and current members of the Schmidt laboratory as well as to Dr. David Gomez-Varela (University of Vienna, Austria) for thoughtful comments on the study. We would like to thank Prof. Dr. Michael Müller (Department of Metabolic and Redox Signaling, UMG, Goettingen, Germany) for sharing the HyPer-mito-YFP plasmid.

This work was supported by the Emmy Noether-Program of the Deutsche Forschungsgemeinschaft (DFG) (SCHM 2533/2-1 to M.S.); the DFG Collaborative Research Center 889 (project A9 to M.S.; project B01 to N.B.); a DFG research grant (PO1319/3-1); the Max Planck Society; the University of Vienna; and a GGNB PhD fellowship (to M.H.). M.S. received research awards and travel support by the German Pain Society (DGSS), both of which were sponsored by Astellas Pharma GmbH (Germany). M.S. received one-time consulting honoraria by Grünenthal GmbH (Germany). During the last 5 years, E.M.P.-Z. received financial support from Mundipharma GmbH and Grünenthal GmbH for research activities and from Grünenthal GmbH, MSD Sharp & DOHME GmbH, Mundipharma GmbH, Mundipharma International, Janssen-Cilag GmbH, Fresenius Kabi Novartis, and AcelRx for advisory board activities and/or lecture fees. Furthermore, this research project was funded by the Ministry for Science and Culture of Lower Saxony and Volkswagen Foundation no. 762-12-9/19 (ZN3457 to S.D.).

AUTHOR CONTRIBUTIONS

D.S., H.K.F., and M.H. performed most experiments and analyzed data unless indicated otherwise. S.D. performed experiments on isolated mitochondria and respective data analysis. F.B. and N.B. generated *Tmem160* KO mice. F.B. developed the genotyping strategy and performed genotyping. D.S. and E.M.P.-Z. designed experiments on mouse behavior. M.S. conceived and directed the study and supervised experiments and data analysis. E.M.P.-Z. supervised behavioral experiments and behavior data analysis and interpreted results. M.S. and D.S. wrote the manuscript and prepared figures with help from H.K.F. and E.M.P.-Z.

DECLARATION OF INTERESTS

The authors declare no competing interests.

Received: January 22, 2021
Revised: September 1, 2021
Accepted: November 30, 2021
Published: December 21, 2021

REFERENCES

Aich, A., Wang, C., Chowdhury, A., Ronsör, C., Pacheu-Grau, D., Richter-Dennerlein, R., Dennerlein, S., and Rehling, P. (2018). COX16 promotes COX2 metallation and assembly during respiratory complex IV biogenesis. eLife *7*, e32572.

Avenali, L., Narayanan, P., Rouwette, T., Cervellini, I., Sereda, M., Gomez-Varela, D., and Schmidt, M. (2014). Annexin A2 regulates TRPA1-dependent nociception. J. Neurosci. *34*, 14506–14516.

Bennett, G.J., Doyle, T., and Salvemini, D. (2014). Mitotoxicity in distal symmetrical sensory peripheral neuropathies. Nat. Rev. Neurol. *10*, 326–336.

Beyer, C., Roberts, L.A., and Komisaruk, B.R. (1985). Hyperalgesia induced by altered glycinergic activity at the spinal cord. Life Sci. *37*, 875–882.

Borsook, D., Hargreaves, R., Bountra, C., and Porreca, F. (2014). Lost but making progress—Where will new analgesic drugs come from? Sci. Transl. Med. *6*, 249sr3.

Callahan, B.L., Gil, A.S.C., Levesque, A., and Mogil, J.S. (2008). Modulation of mechanical and thermal nociceptive sensitivity in the laboratory mouse by behavioral state. J. pain *9*, 174–184.

Cannino, G., El-Khoury, R., Pirinen, M., Hutz, B., Rustin, P., Jacobs, H.T., and Dufour, E. (2012). Glucose modulates respiratory complex I activity in response to acute mitochondrial dysfunction. J. Biol. Chem. *287*, 38729–38740.

Chamessian, A., Matsuda, M., Young, M., Wang, M., Zhang, Z.-J., Liu, D., Tobin, B., Xu, Z.-Z., van de Ven, T., and Ji, R.-R. (2019). Is optogenetic activation of Vglut1-positive Aβ low-threshold mechanoreceptors sufficient to induce tactile allodynia in mice after nerve injury? J. Neurosci. *39*, 6202–6215.

Cicchetti, D.V., and Sparrow, S.A. (1981). Developing criteria for establishing interrater reliability of specific items: applications to assessment of adaptive behavior. Am. J. Ment. Defic. *86*, 127–137.

Claros, M.G., and Vincens, P. (1996). Computational method to predict mitochondrially imported proteins and their targeting sequences. Eur. J. Biochem. *241*, 779–786.

Cobos, E.J., Nickerson, C.A., Gao, F., Chandran, V., Bravo-Caparrós, I., González-Cano, R., Riva, P., Andrews, N.A., Latremoliere, A., Seehus, C.R., et al. (2018). Mechanistic differences in neuropathic pain modalities

revealed by correlating behavior with global expression profiling. Cell Rep. *22*, 1301–1312.

Cook, A.D., Christensen, A.D., Tewari, D., McMahon, S.B., and Hamilton, J.A. (2018). Immune cytokines and their receptors in inflammatory pain. Trends Immunol. *39*, 240–255.

Costigan, M., Scholz, J., and Woolf, C.J. (2009). Neuropathic pain: a maladaptive response of the nervous system to damage. Annu. Rev. Neurosci. *32*, 1–32.

Cunha, A.M., Pereira-Mendes, J., Almeida, A., Guimarães, M.R., and Leite-Almeida, H. (2020). Chronic pain impact on rodents' behavioral repertoire. Neurosci. Biobehav. Rev. *119*, 101–127.

Dahlhamer, J., Lucas, J., Zelaya, C., Nahin, R., Mackey, S., DeBar, L., Kerns, R., Korff, M.V., Porter, L., and Helmick, C. (2018). Prevalence of chronic pain and high-impact chronic pain among adults - United States, 2016. MMWR Morb. Mortal. Wkly Rep. *67*, 1001–1006.

Davis, K.D., Aghaeepour, N., Ahn, A.H., Angst, M.S., Borsook, D., Brenton, A., Burczynski, M.E., Crean, C., Edwards, R., Gaudilliere, B., et al. (2020). Discovery and validation of biomarkers to aid the development of safe and effective pain therapeutics: challenges and opportunities. Nat. Rev. Neurol. *16*, 381–400.

Decosterd, I., and Woolf, C.J. (2000). Spared nerve injury: an animal model of persistent peripheral neuropathic pain. Pain *87*, 149–158.

Dennerlein, S., Oeljeklaus, S., Jans, D., Hellwig, C., Bareth, B., Jakobs, S., Deckers, M., Warscheid, B., and Rehling, P. (2015). MITRAC7 Acts as a COX1-Specific Chaperone and Reveals a Checkpoint during Cytochrome c Oxidase Assembly. Cell Rep. *12*, 1644–1655.

Doench, J.G., Fusi, N., Sullender, M., Hegde, M., Vaimberg, E.W., Donovan, K.F., Smith, I., Tothova, Z., Wilen, C., Orchard, R., et al. (2016). Optimized sgRNA design to maximize activity and minimize off-target effects of CRISPR-Cas9. Nat. Biotechnol. *34*, 184–191.

Doth, A.H., Hansson, P.T., Jensen, M.P., and Taylor, R.S. (2010). The burden of neuropathic pain: a systematic review and meta-analysis of health utilities. Pain *149*, 338–344.

Du Percie Sert, N., and Rice, A.S.C. (2014). Improving the translation of analgesic drugs to the clinic: animal models of neuropathic pain. Br. J. Pharmacol. *171*, 2951–2963.

Dubin, A.E., and Patapoutian, A. (2010). Nociceptors: the sensors of the pain pathway. J. Clin. Invest. *120*, 3760–3772.

Dudek, J., Cheng, I.-F., Chowdhury, A., Wozny, K., Balleininger, M., Reinhold, R., Grunau, S., Callegari, S., Toischer, K., Wanders, R.J., et al. (2016). Cardiac-specific succinate dehydrogenase deficiency in Barth syndrome. EMBO Mol. Med. *8*, 139–154.

Duggett, N.A., Griffiths, L.A., McKenna, O.E., Santis, V.D., Yongsanguanchai, N., Mokori, E.B., and Flatters, S.J.L. (2016). Oxidative stress in the development, maintenance and resolution of paclitaxel-induced painful neuropathy. Neuroscience *333*, 13–26.

Feehan, A.K., and Zadina, J.E. (2019). Morphine immunomodulation prolongs inflammatory and postoperative pain while the novel analgesic ZH853 accelerates recovery and protects against latent sensitization. J. Neuroinflammation *16*, 100.

Flatters, S.J.L. (2015). The contribution of mitochondria to sensory processing and pain. Prog. Mol. Biol. Transl. Sci. *131*, 119–146.

Gereau, R.W., Sluka, K.A., Maixner, W., Savage, S.R., Price, T.J., Murinson, B.B., Sullivan, M.D., and Fillingim, R.B. (2014). A pain research agenda for the 21st century. J. pain *15*, 1203–1214.

Ghasemlou, N., Chiu, I.M., Julien, J.-P., and Woolf, C.J. (2015). CD11b+Ly6G- myeloid cells mediate mechanical inflammatory pain hypersensitivity. Proc. Natl. Acad. Sci. U S A *112*, E6808–E6817.

Glare, P., Aubrey, K.R., and Myles, P.S. (2019). Transition from acute to chronic pain after surgery. The Lancet *393*, 1537–1546.

Grace, P.M., Hutchinson, M.R., Maier, S.F., and Watkins, L.R. (2014). Pathological pain and the neuroimmune interface. Nat. Rev. Immunol. *14*, 217–231.

Guan, Z., Hellman, J., and Schumacher, M. (2016). Contemporary views on inflammatory pain mechanisms: TRPing over innate and microglial pathways. F1000Res. *5*.

Hanack, C., Moroni, M., Lima, W.C., Wende, H., Kirchner, M., Adelfinger, L., Schrenk-Siemens, K., Tappe-Theodor, A., Wetzel, C., Kuich, P.H., et al. (2015). GABA blocks pathological but not acute TRPV1 pain signals. Cell *160*, 759–770.

Holzenberger, M., Lenzner, C., Leneuve, P., Zaoui, R., Hamard, G., Vaulont, S., and Bouc, Y.L. (2000). Cre-mediated germline mosaicism: a method allowing rapid generation of several alleles of a target gene. Nucleic Acids Res. *28*, E92.

Ji, R.-R., Chamessian, A., and Zhang, Y.-Q. (2016). Pain regulation by non-neuronal cells and inflammation. Science *354*, 572–577.

Jirkof, P., Cesarovic, N., Rettich, A., Fleischmann, T., and Arras, M. (2012). Individual housing of female mice: influence on postsurgical behaviour and recovery. Lab. Anim. *46*, 325–334.

Kiguchi, N., Kobayashi, Y., Saika, F., Sakaguchi, H., Maeda, T., and Kishioka, S. (2015). Peripheral interleukin-4 ameliorates inflammatory macrophage-dependent neuropathic pain. Pain *156*, 684–693.

Krames, E.S. (2014). The role of the dorsal root ganglion in the development of neuropathic pain. Pain Med. *15*, 1669–1685.

Lakso, M., Pichel, J.G., Gorman, J.R., Sauer, B., Okamoto, Y., Lee, E., Alt, F.W., and Westphal, H. (1996). Efficient in vivo manipulation of mouse genomic sequences at the zygote stage. Proc. Natl. Acad. Sci. U S A *93*, 5860–5865.

Laumet, G., Ma, J., Robison, A.J., Kumari, S., Heijnen, C.J., and Kavelaars, A. (2019). T Cells as an Emerging Target for Chronic Pain Therapy. Front. Mol. Neurosci. *12*, 216.

Lees, J.G., Duffy, S.S., and Moalem-Taylor, G. (2013). Immunotherapy targeting cytokines in neuropathic pain. Front. Pharmacol. *4*, 142.

Li, J., Ma, J., Lacagnina, M.J., Lorca, S., Odem, M.A., Walters, E.T., Kavelaars, A., and Grace, P.M. (2020). Oral Dimethyl Fumarate Reduces Peripheral Neuropathic Pain in Rodents via NFE2L2 Antioxidant Signaling. Anesthesiology *132*, 343–356.

Liu, X., Tonello, R., Ling, Y., Gao, Y.-J., and Berta, T. (2019). Paclitaxel-activated astrocytes produce mechanical allodynia in mice by releasing tumor necrosis factor-α and stromal-derived cell factor 1. J. Neuroinflammation *16*, 209.

Lopes, D.M., Denk, F., and McMahon, S.B. (2017a). The Molecular Fingerprint of Dorsal Root and Trigeminal Ganglion Neurons. Front. Mol. Neurosci. *10*, 304.

Lopes, D.M., Malek, N., Edye, M., Jager, S.B., McMurray, S., McMahon, S.B., and Denk, F. (2017b). Sex differences in peripheral not central immune responses to pain-inducing injury. Sci. Rep. *7*, 16460.

Mapplebeck, J.C.S., Beggs, S., and Salter, M.W. (2016). Sex differences in pain: a tale of two immune cells. Pain *157*, S2–S6.

McCarson, K.E., and Fehrenbacher, J.C. (2021). Models of inflammation: Carrageenan- or complete Freund's adjuvant (CFA)-induced edema and hypersensitivity in the rat. Curr. Protoc. *1*, e202. https://doi.org/10.1002/cpz1.202.

Meng, J., Wang, J., Steinhoff, M., and Dolly, J.O. (2016). TNFα induces co-trafficking of TRPV1/TRPA1 in VAMP1-containing vesicles to the plasmalemma via Munc18-1/syntaxin1/SNAP-25 mediated fusion. Sci. Rep. *6*, 21226.

Mogil, J.S. (2009). Animal models of pain: progress and challenges. Nat. Rev. Neurosci. *10*, 283–294.

Mogil, J.S. (2012). Sex differences in pain and pain inhibition: multiple explanations of a controversial phenomenon. Nat. Rev. Neurosci. *13*, 859–866.

Mogil, J.S. (2020). The measurement of pain in the laboratory rodent. In The Oxford Handbook of the Neurobiology of Pain, J.N. Wood and J.S. Mogil, eds. (Oxford University Press), pp. 27–60.

Murthy, S.E., Loud, M.C., Daou, I., Marshall, K.L., Schwaller, F., Kühnemund, J., Francisco, A.G., Keenan, W.T., Dubin, A.E., Lewin, G.R., et al. (2018). The

mechanosensitive ion channel Piezo2 mediates sensitivity to mechanical pain in mice. Sci. Transl. Med. *10*.

Nicholls, D.G., and Budd, S.L. (2000). Mitochondria and neuronal survival. Physiol. Rev. *80*, 315–360.

Niehaus, J.K., Taylor-Blake, B., Loo, L., Simon, J.M., and Zylka, M.J. (2021). Spinal macrophages resolve nociceptive hypersensitivity after peripheral injury. Neuron *109*, 1274–1282.e6.

Ono, K., Xu, S., Hitomi, S., and Inenaga, K. (2012). Comparison of the electrophysiological and immunohistochemical properties of acutely dissociated and 1-day cultured rat trigeminal ganglion neurons. Neurosci. Lett. *523*, 162–166.

Pagliarini, D.J., Calvo, S.E., Chang, B., Sheth, S.A., Vafai, S.B., Ong, S.-E., Walford, G.A., Sugiana, C., Boneh, A., Chen, W.K., et al. (2008). A mitochondrial protein compendium elucidates complex I disease biology. Cell *134*, 112–123.

Paldy, E., Simonetti, M., Worzfeld, T., Bali, K.K., Vicuña, L., Offermanns, S., and Kuner, R. (2017). Semaphorin 4C Plexin-B2 signaling in peripheral sensory neurons is pronociceptive in a model of inflammatory pain. Nat. Commun. *8*, 176.

Patapoutian, A., Tate, S., and Woolf, C.J. (2009). Transient receptor potential channels: targeting pain at the source. Nat. Rev. Drug Discov. *8*, 55–68.

Peng, J., Gu, N., Zhou, L., B Eyo, U., Murugan, M., Gan, W.-B., and Wu, L.-J. (2016). Microglia and monocytes synergistically promote the transition from acute to chronic pain after nerve injury. Nat. Commun. *7*, 12029.

Pitzer, C., Kuner, R., and Tappe-Theodor, A. (2016). Voluntary and evoked behavioral correlates in inflammatory pain conditions under different social housing conditions. Pain Rep. *1*, e564.

Pogatzki, E.M., and Raja, S.N. (2003). A mouse model of incisional pain. Anesthesiology *99*, 1023–1027.

Pogatzki-Zahn, E.M., Gomez-Varela, D., Erdmann, G., Kaschube, K., Segelcke, D., and Schmidt, M. (2021). A proteome signature for acute incisional pain in dorsal root ganglia of mice. Pain *162*, 2070–2086.

Price, T.J., Basbaum, A.I., Bresnahan, J., Chambers, J.F., Koninck, Y.D., Edwards, R.R., Ji, R.-R., Katz, J., Kavelaars, A., Levine, J.D., et al. (2018). Transition to chronic pain: opportunities for novel therapeutics. Nat. Rev. Neurosci. *19*, 383–384.

Price, T.J., and Gold, M.S. (2018). From mechanism to cure: Renewing the goal to eliminate the disease of pain. Pain Med. *19*, 1525–1549.

Richardson, C.A., and Flecknell, P.A. (2005). Anaesthesia and post-operative analgesia following experimental surgery in laboratory rodents: are we making progress? Altern. Lab. Anim. *33*, 119–127.

Rosen, S., Ham, B., and Mogil, J.S. (2017). Sex differences in neuroimmunity and pain. J. Neurosci. Res. *95*, 500–508.

Rouwette, T., Sondermann, J., Avenali, L., Gomez-Varela, D., and Schmidt, M. (2016). Standardized profiling of the membrane-enriched proteome of mouse dorsal root ganglia (DRG) provides novel insights into chronic pain. Mol. Cell. Proteomics *15*, 2152–2168.

Schindelin, J., Arganda-Carreras, I., Frise, E., Kaynig, V., Longair, M., Pietzsch, T., Preibisch, S., Rueden, C., Saalfeld, S., Schmid, B., et al. (2012). Fiji: an open-source platform for biological-image analysis. Nat. Methods *9*, 676–682.

Segelcke, D., Pradier, B., Reichl, S., Schäfer, L.C., and Pogatzki-Zahn, E.M. (2021). Investigating the role of Ly6G+ neutrophils in incisional and inflammatory pain by multidimensional pain-related behavioral assessments: Bridging the translational gap. Front. Pain Res. *2*.

Sondermann, J.R., Barry, A.M., Jahn, O., Michel, N., Abdelaziz, R., Kügler, S., Gomez-Varela, D., and Schmidt, M. (2019). Vti1b promotes TRPV1 sensitization during inflammatory pain. Pain *160*, 508–527.

Sorge, R.E., LaCroix-Fralish, M.L., Tuttle, A.H., Sotocinal, S.G., Austin, J.-S., Ritchie, J., Chanda, M.L., Graham, A.C., Topham, L., Beggs, S., et al. (2011). Spinal cord Toll-like receptor 4 mediates inflammatory and neuropathic hypersensitivity in male but not female mice. J. Neurosci. *31*, 15450–15454.

Sorge, R.E., Mapplebeck, J.C.S., Rosen, S., Beggs, S., Taves, S., Alexander, J.K., Martin, L.J., Austin, J.-S., Sotocinal, S.G., Chen, D., et al. (2015). Different immune cells mediate mechanical pain hypersensitivity in male and female mice. Nat. Neurosci. *18*, 1081–1083.

Sorge, R.E., Martin, L.J., Isbester, K.A., Sotocinal, S.G., Rosen, S., Tuttle, A.H., Wieskopf, J.S., Acland, E.L., Dokova, A., Kadoura, B., et al. (2014). Olfactory exposure to males, including men, causes stress and related analgesia in rodents. Nat. Methods *11*, 629–632.

Tansley, S., Uttam, S., Ureña Guzmán, A., Yaqubi, M., Pacis, A., Parisien, M., Rabau, O., Haglund, L., Ouellet, J., Santaguida, C., et al. (2020). Single-cell RNA sequencing reveals time- and sex-specific responses of spinal cord microglia to peripheral nerve injury and links ApoE to neuropathic pain.https://www.biorxiv.org/content/10.1101/2020.12.09.418541v1.

Thakur, M., Crow, M., Richards, N., Davey, G.I.J., Levine, E., Kelleher, J.H., Agley, C.C., Denk, F., Harridge, S.D.R., and McMahon, S.B. (2014). Defining the nociceptor transcriptome. Front. Mol. Neurosci. *7*, 87.

Turner, P.V., Pang, D.S., and Lofgren, J.L. (2019). A Review of Pain Assessment Methods in Laboratory Rodents. Comp. Med. *69*, 451–467.

Tycko, J., Wainberg, M., Marinov, G.K., Ursu, O., Hess, G.T., Ego, B.K., Aradhana, Li, A., Truong, A., Trevino, A.E., et al. (2019). Mitigation of off-target toxicity in CRISPR-Cas9 screens for essential non-coding elements. Nat. Commun. *10*, 4063.

Usoskin, D., Furlan, A., Islam, S., Abdo, H., Lönnerberg, P., Lou, D., Hjerling-Leffler, J., Haeggström, J., Kharchenko, O., Kharchenko, P.V., et al. (2015). Unbiased classification of sensory neuron types by large-scale single-cell RNA sequencing. Nat. Neurosci. *18*, 145–153.

Vasconcelos, M., Hollis, K., Nowbahari, E., and Kacelnik, A. (2012). Pro-sociality without empathy. Biol. Lett. *8*, 910–912.

Vaso, A., Adahan, H.-M., Gjika, A., Zahaj, S., Zhurda, T., Vyshka, G., and Devor, M. (2014). Peripheral nervous system origin of phantom limb pain. Pain *155*, 1384–1391.

Vicuña, L., Strochlic, D.E., Latremoliere, A., Bali, K.K., Simonetti, M., Husainie, D., Prokosch, S., Riva, P., Griffin, R.S., Njoo, C., et al. (2015). The serine protease inhibitor SerpinA3N attenuates neuropathic pain by inhibiting T cell-derived leukocyte elastase. Nat. Med. *21*, 518–523.

Wang, H., Yang, H., Shivalila, C.S., Dawlaty, M.M., Cheng, A.W., Zhang, F., and Jaenisch, R. (2013). One-step generation of mice carrying mutations in multiple genes by CRISPR/Cas-mediated genome engineering. Cell *153*, 910–918.

Wangzhou, A., McIlvried, L.A., Paige, C., Barragan-Iglesias, P., Shiers, S., Ahmad, A., Guzman, C.A., Dussor, G., Ray, P.R., Gereau, R.W., et al. (2020). Pharmacological target-focused transcriptomic analysis of native vs cultured human and mouse dorsal root ganglia. Pain *161*, 1497–1517.

Wetzel, C., Pifferi, S., Picci, C., Gök, C., Hoffmann, D., Bali, K.K., Lampe, A., Lapatsina, L., Fleischer, R., Smith, E.S.J., et al. (2017). Small-molecule inhibition of STOML3 oligomerization reverses pathological mechanical hypersensitivity. Nat. Neurosci. *20*, 209–218.

Willemen, H.L.D.M., Kavelaars, A., Prado, J., Maas, M., Versteeg, S., Nellissen, L.J.J., Tromp, J., Gonzalez Cano, R., Zhou, W., Jakobsson, M.E., et al. (2018). Identification of FAM173B as a protein methyltransferase promoting chronic pain. PLoS Biol. *16*, e2003452.

Yang, H., Wang, H., and Jaenisch, R. (2014). Generating genetically modified mice using CRISPR/Cas-mediated genome engineering. Nat. Protoc. *9*, 1956–1968.

Yang, Y., Luo, L., Cai, X., Fang, Y., Wang, J., Chen, G., Yang, J., Zhou, Q., Sun, X., Cheng, X., et al. (2018). Nrf2 inhibits oxaliplatin-induced peripheral neuropathy via protection of mitochondrial function. Free Radic. Biol. Med. *120*, 13–24.

Yu, X., Liu, H., Hamel, K.A., Morvan, M.G., Yu, S., Leff, J., Guan, Z., Braz, J.M., and Basbaum, A.I. (2020). Dorsal root ganglion macrophages contribute to both the initiation and persistence of neuropathic pain. Nat. Commun. *11*, 264.

Zeisel, A., Hochgerner, H., Lönnerberg, P., Johnsson, A., Memic, F., van der Zwan, J., Häring, M., Braun, E., Borm, L.E., La Manno, G., et al. (2018). Molecular Architecture of the Mouse Nervous System. Cell *174*, 999–1014.e22.

Zhao, D., Han, D.-F., Wang, S.-S., Lv, B., Wang, X., and Ma, C. (2019). Roles of tumor necrosis factor-α and interleukin-6 in regulating bone cancer pain via TRPA1 signal pathway and beneficial effects of inhibition of neuro-inflammation and TRPA1. Mol. pain *15*, 1744806919857981.

Zimmermann, M. (1983). Ethical guidelines for investigations of experimental pain in conscious animals. Pain *16*, 109–110.

Zurborg, S., Piszczek, A., Martínez, C., Hublitz, P., Al Banchaabouchi, M., Moreira, P., Perlas, E., and Heppenstall, P.A. (2011). Generation and characterization of an Advillin-Cre driver mouse line. Mol. pain *7*, 66.

STAR★METHODS

KEY RESOURCES TABLE

REAGENT or RESOURCE	SOURCE	IDENTIFIER
Antibodies		
Chicken anti-peripherin, IgY, polyclonal (1:100)	Abcam	Cat# ab39374; RRID:AB_777207
Donkey anti-goat, Alexa Fluor 488, IgG, polyclonal (1:250, 1:1000)	Life technologies	Cat# A11055; RRID:AB_2534102
Donkey anti-rabbit, Alexa Fluor 488, IgG, polyclonal (1:250)	Life technologies	Cat# A21206; RRID:AB_2535792
Donkey anti-rabbit, Alexa Fluor 680, IgG, polyclonal (1:250)	Life technologies	Cat# A10043 RRID:AB_2534018
Donkey anti-mouse, Alexa Fluor 546, IgG, polyclonal (1:250)	Life technologies	Cat# A10036 RRID:AB_2534012
Goat anti-chicken, Alexa Fluor 555, polyclonal (1:250)	Life technologies	Cat# A21437 RRID:AB_2535858
Goat anti-chicken, Alexa Fluor 647, polyclonal (1:250)	Life technologies	Cat# A21449 RRID:AB_2535866
Goat anti-Tmem160 (N-19), IgG, polyclonal (1:10)	Santa Cruz	Cat# sc-248914
Goat anti-rabbit, Alexa Fluor 488, IgG, polyclonal (1:250)	Life technologies	Cat# A11034 RRID:AB_2576217
Mouse anti-c-Myc, IgG1, monoclonal (1:100)	Life technologies	Cat# 132500 RRID:AB_2533008
Rabbit anti-NDUFV2, IgG, polyclonal (1:100)	Protein Tech	Cat# 15301-1-AP RRID:AB_2149048
Rabbit anti-NF-200, IgG, polyclonal (1:200)	Sigma Aldrich	Cat# N4142 RRID:AB_477272
Rabbit anti-Tmem160, polyclonal (1:10)	Sigma Aldrich	Cat# HPA055904 RRID:AB_2682965
All antibodies directed against mitochondrial proteins employed for western blots	Generated in house; by author SD	N/A
Chemicals, peptides, and recombinant proteins		
Antimycine A	Sigma Aldrich GmbH	Cat# A8674
Betadine®	Avrio Health L.P.	Cat# NDC 67618-155-16
Buprenorphine; TEMGESIC	Essex pharma GmbH	PZN: 0345928
Capsaicin	Sigma Aldrich GmbH	Cat# M2028-50MG
Carprofen; Rimadyl	Zoetis	
Complete Freund's adjuvant	Sigma Aldrich GmbH	Cat# F5881-10ML
cOmplete ULTRA Tablets, Mini, EASYpack	Roche	REF# 05 892 970 001
DMEM/F-12 (1:1) + GlutaMax-I	Gibco	Cat# 31331-028
Donkey Serum	Dianova	SKU: 017-000-121
FCCP	Sigma Aldrich GmbH	Cat# C2920
FuGENE® HD Transfection Reagent	Promega	Cat# E2311
Fura-2/AM	Thermo Fisher Scientific	Cat# F1221
Hanks' Balanced Salt Solution; HBSS (10x)	Gibco	Cat# 14065049
HEPES	Gibco	Cat# 15630056
Horse Serum	Thermo Fisher Scientific	Cat# 16050-122
IRDye 800CW Streptavidin	LI-COR	Cat# 925-32230
Isoflurane	cp-pharma	Cat# 1214
Mustard Oil, AITC	Sigma Aldrich GmbH	Cat# 377430-100G / -5G
NaCl	Merck	Cat# 1064040500
NP40/Igepal	Sigma Aldrich GmbH	Cat# I8896-50ml
NuPAGE 4-12% Bis Tris Gel 1.5mm x 10 well	Thermo Fisher Scientific	Cat# NP0335BOX
Oligomycin B	Sigma Aldrich GmbH	Product# O5126

(*Continued on next page*)

Continued

REAGENT or RESOURCE	SOURCE	IDENTIFIER
Opal 570 dye	Perkin Elmer	Cat# FP1488001KT
Oxygen	Westfalen Gas	UN 1072
PBS (10x)	Thermo Fisher Scientific	Cat# 70011-036
PFA (16%)	Electron Microscopy Sciences	Cat# 15710
Power SYBR Green PCR Master Mix	Thermo Fisher Scientific	Cat# 4368706
QIAzol	QIAGEN	Cat# 79306
RNAscope probe Mm-Tmem160	ACD	Cat# 509071
rhß-NGF	R&D Systems	Cat# 256-GF-100
rhGDNF	R&D Systems	Cat# 212-GD-010
rhNeutrophin-3	R&D Systems	Cat# 267-N3-005
rhNeutrophin-4	R&D Systems	Cat# 268-N4-005
SlowFade Gold Antifade Mountant	Thermo Fisher Scientific	Cat# S36936
SlowFade Gold Antifade Mountant with DAPI	Thermo Fisher Scientific	Cat# S36938
TMRM	Invitrogen/ Life technologies	Cat# T-668
TRIS-HCl	Roth	Cat# 9090.3
TritonX-100	Roth	Cat# 3051.2
Tissue-Tek O.C.T.	Sakura	Cat# 4583
Critical commercial assays		
Complex IV Rodent Enzyme Activity Dipstick Assay Kit	Abcam	Cat# ab109878
NucleoSpin RNA XS Kit	MACHEREY-NAGEL	REF# 740902.50
P3 Primary Cell 4D-Nucleofector X Kit	Lonza	Cat# V4XP-3024
Proteome Profiler Mouse Cytokine Array Kit, Panel A	R&D Systems	Cat# ARY006
QuantiTectReverse Transcription Kit	QIAGEN	Cat# 205311
RNAscope Multiplex Fluorescent Reagent Kit v2	ACD	Cat# 323100
RNeasy Mini Kit	QIAGEN	Cat# 74104
Experimental models: Cell lines		
HEK293T	ATCC	CRL-3216
Experimental models: Organisms/strains		
C57BL/6J (*M. musculus*)	Jackson Lab	RRID: IMSR_JAX:000664
EIIa-Cre (M. musculus)	Jackson Lab	B6.FVB-Tg(EIIa-cre)C5379Lmgd/ J Stock No: 003724
Tmem160 KO (*M. musculus)*	Generated in house, see STAR Methods	N/A
Advillin-Cre (M. musculus)	Kind gift of Prof. Dr. Klaus-Armin Nave, MPIEM, Göttingen	(Zurborg et al., 2011) Tg(Avil-cre) 1Phep MGI:5292346
Oligonucleotides		
Primers for genotyping and qPCR	Generated in house	Table S1
Recombinant DNA		
HyPer-mito-YFP	Kind gift from Prof. Dr. Michael Müller, UMG Goettingen	N/A
pCDNA3.1-myc-His	Invitrogen	Cat# V80020
pCMV6-TMEM160-Myc-DDK	Origene	CAT# PS100007
Software and algorithms		
Adobe Illustrator®	https://www.adobe.com/de/products	RRID:SCR_010279
Adobe Photoshop	Adobe Systems	RRID:SCR_04199
Axiovision	Zeiss	RRID:SCR_002677
Boris	http://www.boris.unito.it/	RRID: SCR_021434

(*Continued on next page*)

Continued

REAGENT or RESOURCE	SOURCE	IDENTIFIER
GraphPad Prism 8	www.graphpad.com/scientific-software/prism	RRID: SCR_015807
ImageJ	https://imagej.net/Fiji	RRID: SCR_003070
MetaFluor	Molecular Devices	RRID:SCR_014294
Microsoft 365®	https://www.microsoft.com/	RRID:SCR_014001
SPSS	IBM	RRID:SCR_002865
Other		
5-0 PROLENE®	Ethicon	Cat# 8205H
6-0 PROLENE®	Ethicon	Cat# EH7400H
Axio Observer Z1	Zeiss	RRID:SCR_021351
CatWalk™ XT gait system	Noldus	RRID:SCR_021262
Cryostat	Leica	RRID:SCR_002865
Hargreaves radiant heat apparatus	IITC Life Science	RRID:SCR_012152
Lightcycler 480	Roche	RRID:SCR_020502
Microsyringe	Hamilton	N/A
4D- Nucleofector X Unit	Lonza	Cat# AAF-1002X
Odyssey Infrared Imaging System	LI-COR	N/A
Plantar Aesthesiometer	Ugo Basile	RRID:SCR_021751
Precellys Homogenisator	Bertin Instruments	N/A
Seahorse XF Analyzer	Seahorse Bioscience	RRID:SCR_019540
SuperFrostPlus™ slides	Thermo Fisher Scientific	Cat#10149870
Von Frey filaments	Bioseb	Cat# Bio-VF-M

RESOURCE AVAILABILITY

Lead contact

Further requests for resources should be directed to and will be fulfilled by the lead contact, Manuela Schmidt (manuela_schmidt@univie.ac.at).

Materials availability

The Tmem160 KO mouse line generated in this study is available on request.

Data and code availability

- The published article includes all behavior datasets generated and analyzed during the course of this study. All other original data, western blot images, and microscopy images will be shared by the lead contact upon request.
- This paper does not report original code.
- Any additional information required to reanalyze the data reported in this paper is available from the lead contact upon request.

EXPERIMENTAL MODEL AND SUBJECT DETAILS

Mice

Adult C57BL/6J mice of both sexes at the age of 10-14 weeks were used for behavioral and molecular biology studies. Mice were group-housed in sex- and age-matched ventilated cages (2 to 5 per cage) under a 12 h (h)- light/12h-dark cycle with ad libitum access to water and food in one room under standardized conditions. All experiments involving mice were performed in observation of ARRIVE guidelines and by approval of the MPIEM institutional animal care and use committee (IACUC), the Animal Ethics Committee of the State Agency for Nature, Environment and Consumer Protection North Rhine-Westphalia (LANUV, Germany; registration number: 81-02.04.2017.A491) and the Landesamt für Verbraucherschutz und Lebensmittelsicherheit of Lower Saxony (LAVES, Germany; registration number: Az 17/2501 und Az 13/1359). All animal procedures were conducted in accordance with the ethical guidelines for the investigation of experimental pain in conscious animals (Zimmermann, 1983).

Generation and validation of Tmem160 knockout (KO) mice

Generation of *Tmem160* KO mice was accomplished by CRISPR/Cas9 technology (Wang et al., 2013; Yang et al., 2014). Superovulated C57Bl/6JRj females (3-4 w) [pregnant mare; serum gonadotropin (7.5 U, Pregmagon, IDT Biologika GmbH, Germany) and human chorionic gonadotropin (5 U, Ovogest, MSD Animal Health)] were mated with C57Bl/6JRj males and fertilized eggs collected. To flank exon 1 with loxP sites (Figure 1A, Allele: *Tmem160 floxed*) in-house made CRISPR reagents (hCAS9_sgRNAs_HDR.DNA; 1 gRNA/loxP site; one long dsDNA as repair template) were microinjected into the pronucleus and the cytoplasm of zygotes at the pronuclear stage using an Eppendorf Femtojet. Note that all gene-specific reagents (i.e., sgRNAs and hCAS9) were used as RNA molecules and were not plasmid-coded. In this way, we intended to reduce the likelihood for off-target effects, as RNA-based reagents are only short-lived (Doench et al., 2016; Tycko et al., 2019) in contrast to plasmid-coded reagents. Accordingly, the CFD specificity score was 96 out of 100 (sgRNA1) and 92 out of 100 (sgRNA2), indicating a very low probability for off-target effects (Doench et al., 2016; Tycko et al., 2019).

Zygotes were transferred bilaterally in the oviducts of pseudopregnant NMRI fosters. Global (constitutive) *Tmem160* KO mice were generated by crossing floxed *Tmem160* mice with an *EIIaCre* driver line (Lakso et al., 1996; Holzenberger et al., 2000) (recombination at E0.5). Successful global deletion of *Tmem160 (*Allele: *Tmem160 recombined, KO)* was confirmed by genotyping according to standard PCR methods using DNA isolated from tail biopsies, quantitative reverse transcription PCR (qPCR with primers directed against exon 2 and exon 3 of *Tmem160* mRNA; for detailed procedure and primers please see below), and in situ hybridization using RNAscope technology (Figure 1B; RNAscope probe Mm-Tmem160 targets region 2-819 of *Tmem160* mRNA, ACD, Cat No. 509071). *Tmem160* KO mice were healthy and fertile. Tmem160 conditional KO (cKO) mice, in which Tmem160 was deleted in the majority of sensory neurons of DRG, were generated by crossing floxed Tmem160 mice with the Advillin-Cre driver line (Zurborg et al., 2011). Tmem160 cKO mice were healthy and fertile.

Successful deletion of Tmem160 was confirmed by genotyping according to standard PCR methods using DNA isolated from tail biopsies (using the Genomic DNA Isolation Kit for Tissue and Cells according to the manufacturer's protocol; Nexttec, Hilgertshausen, Germany). For quality control, all samples were analyzed on a 1% agarose gel. Genotyping primers and fragment sizes are listed in Table S1. In addition, we used quantitative reverse transcription PCR to confirm the successful deletion of Tmem160 mRNA in DRG (qPCR with primers directed against exon 2 and exon 3 of Tmem160 mRNA; for detailed procedure and primers, please see below and Table S1).

Dissociated cultures of DRG neurons

Primary cultures of mouse DRG neurons were prepared as described previously (Sondermann et al., 2019). Neurons were cultured up to 24 h in culture medium (DMEM/F-12 (1:1) + GlutaMax-I, Gibco™, Thermo Fisher Scientific, MA USA) with 10 % horse serum (Thermo Fisher Scientific, MA USA) and NGF (100 ng/mL; R&D Systems, Germany). Genotype and sex of cells are indicated in the respective figure legend.

HEK293T cell culture and transfection

HEK293T cells were originally authenticated by ATCC (Manassas, USA) upon purchase. Thereafter, cell line identity was authenticated by regular morphological inspection. Symptoms for mycoplasma contamination were not observed and thus no test for mycoplasma contamination was performed. HEK293T cells were cultured and transfected as described previously (Sondermann et al., 2019). In brief, HEK293T cells were cultured in DMEM + Glutamax + 10 % FBS + 1 % penicillin/streptomycin (all Thermo Fisher Scientific, MA USA).

METHOD DETAILS

Pain models

Acute Pain: Mice were acclimatized to the testing chamber for 1h. Mice were unilaterally injected with the TRPA1-agonist mustard oil (50 mM in 1x PBS, volume: 10 μL, Sigma-Aldrich GmbH, Germany) or the TRPV1-agonist capsaicin (0.5 μg in 5% EtOH/1x PBS, volume: 10 μL, Sigma-Aldrich GmbH, Germany) into the hindpaw as described previously (Avenali et al., 2014; Sondermann et al., 2019). For acute pain behavior assessment, the time the mouse spent lifting, licking or flicking the injected paw was measured. Afterwards, tactile hypersensitivity was assessed with a Plantar Aesthesiometer (Ugo Basile R&D SA, Swiss) up to 90 min (min) post-injection. The device was adjusted to deliver stimuli with the following parameters: increasing force up to 10 g within 40 s (s). The withdrawal latency and force were recorded five times for each animal's hind paw within a 30 min timeframe with at least 3 min intervals between stimuli. Mice were sacrificed after the experiment.

Paw incision-model (INC): Incisional pain was performed similar as described by us before (Pogatzki and Raja, 2003); briefly, all mice were initially anesthetized with 5% isoflurane (in 100% oxygen, UN 1072, Westfalen Gas, Germany) and maintained with 1.5-2% isoflurane (1 ml/ml, veterinary, cp-pharma, Germany) via a nose cone. Sterility was maintained throughout the entire surgical procedure. Paw incision was performed by 0.5 cm longitudinal incision was made through glabrous skin and fascia of the plantar aspect of the right hind paw; the underlying musculus digitorum brevis was incised longitudinally (Scalpel No 11) while taking care not to affect the site of muscle insertion. The skin was closed with one mattress suture of 6-0 PROLENE® (Ehticon Inc., NJ USA) and covered by Betadine® (Avrio Health L.P., USA). Sutures were removed postoperatively on day 3 under short isoflurane

anesthesia. The Incision-control group was represented by sham-treated mice (only anesthesia, same exposure duration, no incision).

CFA-model: Pathogen- and adjuvant-induced inflammatory pain was initiated by injecting 20 μl complete Freund's adjuvant (CFA, Sigma-Aldrich GmbH, Germany) subcutaneously (s.c.) into the plantar aspect of the right hindpaw with a 27-gauge Hamilton microsyringe (Ghasemlou et al., 2015). Sham-treated animals received s.c.-application of sterile 0.9% saline (20 μl) in the same aspect of the hindpaw.

SNI-model: Neuropathic pain was induced by nerve injury of common peroneal and tibial nerves (Decosterd and Woolf, 2000). This partial denervation model (spared nerve injury, SNI) produces reliable and reproducible tactile hypersensitivity in the dermatome of spared, intact sural nerve. Thirty min prior to the surgery, buprenorphine (0.07 mg/kg, s.c., TEMGESIC, 0.3 mg injection solution, Essex pharma GmbH, Germany) was applied to relieve acute pain (Richardson and Flecknell, 2005). All mice were initially anesthetized with 5% isoflurane (in 100% oxygen, UN 1072, Westfalen Gas, Germany) and maintained with 1.5-2% isoflurane (1 ml/ml, veterinary, cp-pharma, Germany) via a nose cone. Following skin incision above the biceps femoris muscle, blunt dissection was performed to expose the trifurcation of the sciatic nerve. A ligature with 8-0 silk surgical knot was created under common peroneal and tibial nerves. Both nerves were transected distally (2 mm nerve section was removed to prevent regeneration). Using 5-0 PROLENE®, the skin was closed with three single sutures and covered by Betadine® (Avrio Health L.P., USA). Sutures were removed postoperatively on day 5 under short isoflurane anesthesia. The SNI-control group (SNI-Sham) was performed in the same way without ligature and transection branches of the sciatic nerve. Postoperative analgesia consisted of daily application of carprofen (Rimadyl®, Zoetis, Germany) for a maximum of three days (5 mg/kg, s.c.).

Behavior assays upon INC, CFA-injection and SNI

Behavioral assessments were performed between 8 am, and 12 am by randomly selected experimenters of both genders and in a blinded-manner concerning genotype and, in case of SNI, the pain model (blinding is not possible for INC and CFA given the visible incision suture and visible paw inflammation, respectively). The experimental groups were assembled randomly (Microsoft® Excel random list). Mice were accustomed to testing apparatus daily for at least 4 days before "pre" (baseline) testing. For testing the tactile hypersensitivity, we used a set of calibrated von Frey filaments (Bioseb, France) with a logarithmic force range from 0.07 g to 2 g, presented perpendicularly 5 times (1Hz) to the plantar aspect of the ipsilateral hindpaw. In this way, the ascending stimulus method determined the 60% paw withdrawal threshold (Mogil, 2020). Heat hypersensitivity was assessed using the Hargreaves radiant heat apparatus (IITC Life Science, Halogen lamp intensity 17%, Temperature test platform, 30°C) by determining the paw withdrawal latency time (in seconds) with a cut-off time of 20 s to prevent tissue damage. The precise location of stimuli on the hindpaw was dependent on the pain model (mid-plantar aspect for INC and CFA, sural nerve skin territory for SNI). Movement-evoked pain-related behavior was determined by CatWalk^{TM} XT gait system (Noldus, Netherlands). Each mouse was repeatedly placed on the horizontal walkways to complete three uninterrupted runs in a voluntary manner in max 5 s and 60% speed variation per run. Analyses of these recordings yielded many parameters, of which the following have been the most acknowledged and applied in pain models (Pitzer et al., 2016; Feehan and Zadina, 2019): Stand time and print area as static gait parameters, and swing speed and duty cycle as dynamic gait parameters. These parameters have been shown to be suitable to quantify the expression of the antalgic (avoidance) volunteer gait caused by unilateral injury in rodent pain models (Pitzer et al., 2016; Feehan and Zadina, 2019; Segelcke et al., 2021). Non-evoked pain behavior (NEP) was measured by analysis of the mean print area of both hind paws in rest over 10 min (Pogatzki-Zahn et al., 2021; Segelcke et al., 2021). Briefly, mice were placed on a 1 cm thick Plexiglas plate and covered with a transparent plastic box (5 x 10 cm) from above. A video (10 min) was recorded from below, based on which the print area of each hindpaw was calculated from 20 selected fixed-images (one for every 30 s) using ImageJ Fiji (Schindelin et al., 2012). Screenshots were created in a blinded manner concerning the pain model and genotype. Using ImageJ, the contact surface of the right (ipsilateral) hind paw was analyzed in relation to the left (contralateral) hind paw. Images were considered poor quality and thus excluded if mice were rearing, twisting, not all paws were on the ground, or excessive urination was present below the hind paws. Mice were excluded if less than three images out of the 20 images were of good quality. To eliminate increasing body weight over the experimental period as a confounding factor, all parameters of locomotion and NEP are expressed as the ratio between the right (ipsilateral, treated) and left (contralateral) hindpaw.

In addition to pain-related behaviors, we addressed changes in pain-related self-grooming potentially implicated in hypoalgesia (Callahan et al., 2008). Self-grooming was represented by bouts of wiping, licking, and nibbling the fur with forepaws and tongue (Jirkof et al., 2012). Self-grooming was recorded during the NEP measurement and analyzed manually for its frequency and duration. This analysis was performed by two independent experimenters in a blinded manner regarding pain model, genotype, sex, and time with "Behavioral Observation Research Interactive Software" (BORIS, https://www.boris.unito.it/).

Nucleofection of dissociated DRG neurons

The P3 Primary Cell 4D-Nucleofector X Kit (Lonza, Switzerland) was used to nucleofect dissociated DRG neurons in the 4D-Nucleofector X Unit (Lonza, Switzerland) essentially as described previously (Sondermann et al., 2019). The following plasmids were used: 0.5 μg pCMV6-TMEM160-Myc-DDK (purchased from Origene) or pCDNA3.1-myc-His (control transfection for anti-Myc labeling specificity, data not shown) in combination with 0.5 ug HyPer-mito-YFP. Nucleofected neurons were cultured in DMEM/F-12 + Glu-

tamax + 10 % horse serum + 100 ng/ml NGF + 50 ng/ml GDNF + 50 ng/ml NT-3, and 50 ng/ml NT-4 (all growth factors were procured from R&D Systems, Germany). At 2 DIV (days *in vitro*) neurons were used for immunocytochemistry.

HEK293T cell culture and transfection

HEK293T cells were cultured and transfected as described previously (Sondermann et al., 2019). In brief, HEK293T cells were cultured in DMEM + Glutamax + 10 % FBS + 1 % penicillin/streptomycin (all Thermo Fisher Scientific, MA USA). Human Tmem160-FLAG (Figures S1B and S1C) was transfected using GenJuice transfection reagent, following the manufacturers' protocol. The transfection of 0.5 μg pCMV6-TMEM160-Myc-DDK or pCDNA3.1-myc-His was performed using FuGENE (Promega, Germany) according to the manufacturerś protocol. At 2 DIV cells were used for immunocytochemistry.

Ca^{2+}-imaging

Ratiometric Ca^{2+}-imaging was performed on cultured DRG neurons at 1DIV essentially as described previously (Sondermann et al., 2019). Briefly, coverslips were washed with warm assay buffer (1x Hanks' Balanced Salt Solution (1.3 mM Ca^{2+}) with 10 mM HEPES, ThermoFisher Scientific, MA USA), incubated with 2.5 μM Fura-2/AM (ThermoFisher Scientific, MA USA) in assay buffer (30 min, 37°C, 5% CO_2) and transferred to a recording chamber, perfused (gravity-driven) with assay buffer, and imaged at room temperature (RT) at an inverted microscope (Zeiss Axio Observer Z1, Germany) by alternating excitation at 340 nm and 380 nm and acquisition at 510 nm using MetaFluor software (Molecular Devices, San José, CA USA). Two different stimulation protocols were performed as indicated in Figures 5 and S7. Data analysis. For each neuron, a baseline was calculated prior to each stimulus as the mean 340/380 ratio over a period of 15 s prior to stimulation. Within this range, amplitudes were calculated as the maximum 340/380 ratio per responder subtracted by the respective baseline. Responders were defined as cells with maximum amplitude values reaching 120% of the respective baseline within the time span from response onset over the duration of the stimulus (one or two min). Neurons with unstable recordings (high variation of the baseline) were excluded from further analysis. At least two coverslips per condition from three to four independent culture preparations were analyzed.

Real-time quantitative PCR (qPCR)

Real-time quantitative PCR experiments were performed as described previously (Sondermann et al., 2019). In brief, total RNA was extracted from cell lysates of *Tmem160* KO mice and wildtype littermates using different methods depending on the tissue type. RNA from DRG was isolated using the NucleoSpin RNA XS kit (MACHEREY-NAGEL, Düren, Germany) according to the manufacturer's instructions. RNA from the spinal cord and sciatic nerve was isolated using Qiazol (QIAGEN, Germany), homogenized with a Precellys Homogenisator (5000 rpm, 3x10 s), Chloroform extracted, and finally applied to an RNeasy Mini Spin Column according to the instructions of the RNeasy Mini Kit (QIAGEN, Germany). QuantiTect Reverse Transcription Kit (QIAGEN, Germany) was used to create cDNA following the manufacturer's instructions. The real-time qPCR for comparative gene expression analysis was performed on a Lightcycler 480 platform (Roche, Rotkreuz, Switzerland) with SYBR™ Green fluorescence detection using the Power SYBR Green PCR Master Mix (ThermoFisher Scientific, MA USA). A final melting curve analysis confirmed the specificity of the amplified product. The threshold cycle (Ct) values – the cycle number at which SYBR™ Green fluorescence exceeded the background – were taken as a measure of initial transcript amount and normalized to the reference gene GAPDH. Data analysis: For each sample, the mean Ct-value was determined per triplicate. If the standard deviation was higher than 0.2, the most deviant value from the mean was excluded, and a mean of the two remaining Ct-values was considered. If the standard deviation was higher than 1.0, all triplicate samples were excluded from further analysis. After generating a mean value for each sample and each gene, all Ct-values were normalized to GAPDH (housekeeping gene), considered an indicator of the total amount of mRNA present in the initial tissue sample. ΔCt-values were generated for each gene and sample by normalization to GAPDH. Then, ΔCt-values were compared between conditions (ipsilateral and contralateral sides) and genotypes with the $2^{-\Delta\Delta Ct}$ method. For all qPCR experiments, ΔCt-values were only considered if conditions or genotypes to be compared yielded high-quality data (see above) within the same experimental round to ensure parallel processing of biological replicates. Sequences of primers are listed in Table S1.

Immunocytochemistry (ICC)

At 2 DIV HEK293T cells or nucleofected DRG cultures were washed in 1x PBS (ThermoFisher Scientific, MA USA) and subsequently fixed in 4 % PFA (Electron Microscopy Sciences) for 10 min at RT. After several washes in 1x PBS cells were incubated with blocking solution (5 % donkey serum (Dianova, Germany), 0.4 % Triton® X-100 (Roth, Germany) in 1x PBS) for 30 min at RT and thereafter with primary antibodies (diluted in 1 % donkey serum, 0.1 % Triton® X-100 in 1x PBS) at 4°C overnight. After several washes in 1x PBS, cells were incubated with respective secondary antibodies (diluted in 1 % donkey serum, 0.1 % TritonX-100 in 1x PBS) for 2h at RT. Finally, coverslips were washed several times in 1x PBS and mounted with Slowfade gold antifade reagent (ThermoFisher Scientific, MA USA). At least two to three independent culture preparations were analyzed. Primary antibodies: NDUFV2 (Protein Tech, Rabbit, 1:100), c-Myc (LifeTechnologies, CA USA, Mouse, 1:100). Secondary antibodies: Alexa Fluor 488 α rabbit (LifeTechnologies, CA USA, Donkey, 1:250), Alexa Fluor 546 α mouse (LifeTechnologies, CA USA, Donkey, 1:250), Alexa Fluor 488 α goat (Life Technologies, CA USA, Donkey, 1:250, 1:1000).

Immunohistochemistry

Mice were euthanized by CO_2-inhalation and lumbar DRG from levels 1-5 dissected. Tissues were fixed in 4 % PFA (Electron Microscopy Sciences Fisher Scientific, Germany)/ PBS at 4°C for 24h followed by cryoprotection in 30% sucrose (Merck)/ PBS at 4°C overnight. Subsequently, tissue was frozen in Tissue-Tek O.C.T. (Sakura Finetek, Torrance, CA USA). Step-serial sections of 10 μm thickness were cut with a cryostat (Leica, Wetzlar, Germany), mounted on SuperFrost Plus slides (Thermo-Fisher Scientific, MA USA), and stored at -80°C until further use. Frozen tissue sections were thawed, surrounded by a fat pen, and treated for 1 h with blocking buffer (5 % donkey serum (Dianova), 0.4 % TritonX-100 (Roth, Germany) in 1x PBS) at RT. Afterwards, slides were incubated with primary antibodies (diluted in 1 % donkey serum, 0.1 % TritonX-100 in 1x PBS) at 4°C overnight. After several washes in 1x PBS slides were incubated with respective secondary antibodies (diluted in 1 % donkey serum, 0.1 % Triton® X-100 in 1x PBS) for 2h at RT. Finally, slides were washed several times in 1x PBS and mounted with Slowfade gold antifade reagent with or without DAPI (ThermoFisher Scientific, MA USA). All incubation steps were performed in a humid chamber. Secondary Ab controls (omission of primary antibody) were performed to control for unspecific background staining. Primary antibodies: Peripherin (Abcam, Chicken, 1:100), NF-200 (Sigma-Aldrich, Germany, Rabbit, 1:200), unspecific Tmem160 antibodies (Tmem160 (Sigma-Aldrich, Germany, Rabbit,1:10) Tmem160 (N-19, Santa Cruz, TX USA, Goat, 1:10)). Secondary antibodies: Alexa Fluor 488 α rabbit (Invitrogen, Goat, 1:250), Alexa Fluor 488 α rabbit (Life Technologies, CA USA, Donkey, 1:250), Alexa Fluor 488 α Goat (Life Technologies, CA USA, Donkey, 1:250), Alexa Fluor 555 α Chicken (Life Technologies, CA USA, Goat, 1:250), Alexa Fluor 647 α Chicken (Invitrogen, MA USA, Goat, 1:250), Alexa Fluor 680 α rabbit (Life Technologies, CA USA, Donkey, 1:250).

Image acquisition and analysis

For all immunostainings, digital images were acquired on a Zeiss Axio Observer Z1 inverted epifluorescence microscope with Axiovision software (Zeiss, Oberkochen, Germany) and analyzed as described previously (Sondermann et al., 2019). The acquisition parameters were kept constant for all experimental groups and all controls. All conditions to be compared were processed in parallel. Raw images were analyzed by using ImageJ Fiji (Schindelin et al., 2012). Neurons were considered as immuno-label positive if their mean intensity (in arbitrary units) exceeded the mean background intensity + 3× standard deviation from at least 10 random unstained cells. To avoid double-counting of neurons, only sections that were at least 50 μm apart were considered. Only for presentation purposes were brightness & contrast of matched images adjusted (always in parallel) with ImageJ Fiji (Schindelin et al., 2012) or Adobe Photoshop CC2017 (Adobe Systems, CA USA).

Cytokine array

DRG of all levels were isolated from mice as described above and snap-frozen in liquid nitrogen. DRG from two mice of the same genotype were pooled and lysed in a tissue grinder using freshly prepared lysis buffer (20 mM TRIS-HCl (Roth, Germany), 137 mM NaCl (Merck, Germany), 1% Glycerol (Roth, Germany), one tablet protease inhibitor (Roche, Switzerland), 1% NP40/Igepal (Sigma-Aldrich) and 1% TritonX-100 (Roth, Germany)) at 4°C for 1 h. Subsequently, lysates were centrifuged at 2500 x g at 4°C for 10 min. Protein concentrations in the supernatant of each sample were determined in a spectrophotometer and, in addition, by gel-electrophoresis via 1D NuPAGE® (ThermoFisher Scientific, MA USA) and subsequent Coomassie Staining. The Proteome Profiler Mouse Cytokine Array Kit, Panel A (R&D Systems, MI USA) was used to compare cytokine and chemokine levels in DRG lysates between KO and WT littermates according to the manufacturerś instructions. Lysates (with similar total protein content) from KO and WT littermates/sex were always assayed in parallel to facilitate relative quantification. Proteome Profiler membranes were incubated with 0.5 μg/ml IRDye 800CW Streptavidin (LI-COR Biosciences, NE USA) and imaged using a LI-COR Odyssey Infrared Imaging System (wavelength/channel: 800 nm, resolution: 169 μm, intensities: 3.0, quality: high). Three independent experiments were performed, i.e., in total N=6 animals on n=3 membranes were used per genotype and sex. Data analysis: Any speckles on the membrane were excluded from the analysis. Each cytokine and chemokine to be analyzed is spotted in duplicates on Proteome Profiler membranes (Figure S6). The mean pixel intensity of each spot was measured using ImageJ Fiji (Schindelin et al., 2012) and corrected with the background intensity. Thereafter, the mean intensity per duplicate was calculated and corrected for differences in input amounts, if necessary. To this end, images of aforementioned Coomassie-stained protein gels were used. For each sample, the same five stained protein bands across the whole molecular weight range were selected, and their mean pixel intensity was calculated. The mean pixel intensity of the background was subtracted, and the resulting values of all five bands per sample were summed up and compared between KO and WT samples (for each sex separately). If KO and WT input differed more than 8 %, this difference was used as a correction factor of the mean intensity per duplicates in the Proteome Profiler Array. This facilitated the quantification of relative cytokine and chemokine levels in KO samples normalized to respective controls.

RNAscope

The RNAscope® Multiplex Fluorescent Reagent Kit v2 (ACD, CA USA) was used to validate the global knockout of *Tmem160* and to assess the distribution of *Tmem160 mRNA* in DRG of WT mice (RNAscope probe Mm-Tmem160, ACD CA USA,). The method was performed according to the manufacturerś instructions for fixed frozen tissue adapted to procedure above of tissue embedding and cryosectioning. Manual target retrieval was performed for 5 min. For the HRP-C1 signal, an Opal 570 dye (PerkinElmer, Germany)

(1:1500 in TSA buffer) was used. After the addition of HRP blocker, a standard IHC was performed basically as described above. Slides were mounted with ProLong Gold Antifade Mountant with DAPI (ThermoFisher Scientific, MA USA) and imaged until two weeks later. Digital images were acquired on a Zeiss Axio Observer Z1 inverted epifluorescence microscope with Axiovision software (Zeiss, Germany). All conditions to be compared were processed and imaged in parallel using identical settings. Only for presentation purposes were brightness & contrast of matched images adjusted (always in parallel) with ImageJ Fiji (Schindelin et al., 2012) or Adobe Photoshop CC2017 (Adobe Systems, CA USA).

TMRM imaging

TMRM (Nicholls and Budd, 2000; Cannino et al., 2012) (tetramethylrodamine, methyl ester, Invitrogen) was used to assess potential mitochondrial dysfunction. DRG cultures, generated as described above, were incubated with 3 nM TMRM in assay buffer (1x Hanks' Balanced Salt Solution (1.3 mM Ca^{2+}) with 10 mM HEPES, ThermoFisher Scientific, MA USA) for 1 h at RT. Following, neurons were imaged every 20 s for 6 min: 2 min baseline (assay buffer + 3 nM TMRM), 2 min 1 μM FCCP (mitochondrial oxidative phosphorylation uncoupler, Sigma-Aldrich; in assay buffer + 3 nM TMRM), 2 min washout (assay buffer). Digital images were acquired on a Zeiss Axio Observer Z1 inverted epifluorescence microscope with Axiovision software (Zeiss, Germany). All conditions to be compared were processed and imaged in parallel using identical settings. For analysis, the TMRM mean intensity after the addition of FCCP was normalized to the baseline. Only neuronal axons were considered for analysis, given saturated signals from neuronal somata. At least 4 regions of interest/image, 12 images/coverslip, and 3 coverslips per independent experiment and genotype were analyzed with ImageJ Fiji (Schindelin et al., 2012). At least 3 independent culture preparations were analyzed. Only for presentation purposes were brightness & contrast of matched images adjusted (always in parallel) with ImageJ Fiji (Schindelin et al., 2012) or Adobe Photoshop CC2017 (Adobe Systems, CA USA).

Complex IV rodent enzyme activity dipstick assay

To quantify the activity of the Cytochrome C Oxidase (COX) enzyme complex (Complex IV of mitochondrial electron transport chain) the Complex IV Rodent Enzyme Activity Dipstick Assay Kit (Abcam, UK) was used according to the manufacturer's instructions. The assay was performed on isolated non-dissociated DRG (IDRG and DRG from all levels) in triplicates. Images of dipsticks were acquired with a digital camera, and their mean pixel intensity was analyzed with ImageJ Fiji (Schindelin et al., 2012). At least three independent experiments were performed in triplicates. Only for presentation purposes were brightness & contrast of matched images adjusted (always in parallel) with ImageJ Fiji (Schindelin et al., 2012) or Adobe Photoshop CC2017 (Adobe Systems, CA USA).

Seahorse respiration of isolated mitochondria

Isolation of mitochondria was performed as described previously (Dennerlein et al., 2015; Aich et al., 2018). Mouse brain tissue was thoroughly homogenized in TH buffer (10 mM KCl, 10 mM Hepes-KOH (pH 6.9), 300 mM Trehalose) with BSA (0.1 %) followed by centrifugation (10 min, 4°C, 400 x g) and collection of supernatants. The homogenate was resuspended in TH buffer with BSA. Subsequently, the samples were homogenized again, and the suspension was centrifuged (10 min, 4°C, 400 x g). Supernatants were collected and centrifuged (5 min, 4°C, 800 g, and 10 min, 4°C, 10,000 x g), resulting in the formation of a mitochondria-containing pellet. The pellet was resuspended in TH buffer without BSA and centrifuged (5 min, 4°C, 10,000 x g). The resulting pellet was resuspended in TH buffer, and protein concentrations were assessed with the Bradford assay (BSA was used as standard). Mitochondrial respiration (oxygen consumption rate, OCR) and glycolysis (extracellular acidification rate, ECAR) was measured using the Seahorse XF Analyzer (Seahorse Bioscience, Billerica, MA USA) as described previously (Dudek et al., 2016). The following drugs were applied in the support plate: Oligomycin (4 μM, Sigma-Aldrich), FCCP (2 μM, Sigma-Aldrich, Germany), Antimycin (2 μM, Sigma-Aldrich, Germany), Rotenone (2 μM, Sigma-Aldrich, Germany), and KCN (1 mM, Fluka). Drugs were kept at 4°C and equilibrated to 37°C 15 min before the experiment was started. Upon detecting a drop in O_2 or H^+ by raising the sensor cartridge, the baseline was allowed to restore. Isolated mitochondria were loaded (10x, 18 μl) into the chilled cell plate and spun down (20 min at 4°C). Afterwards, the instrument was equilibrated, mitochondrial assay solution (70 mM sucrose, 220 mM mannitol, 2 mM HEPES, 10 mM KH2PO4, 5 mM MgCl2, 1 mM EGTA, 0.2 % BSA) was pipetted into each well (162 μl), and measurements were started.

Tmem160 localization assays in isolated mitochondria

Carbonate extraction and mitochondrial swelling experiments were performed on isolated mitochondria from HEK293T cells as previously described (Dennerlein et al., 2015; Aich et al., 2018). In brief, to conduct carbonate extraction of proteins, isolated mitochondria were incubated in 100 mM Na_2CO_3 (pH 10.8 or 11.5) and then centrifuged (30 min, 100,000 x g, 4°C). Protease protection assay using proteinase K (PK) was performed to assess the submitochondrial localization of human Tmem160-Flag protein and reference proteins (Figure S1). Isolated mitochondria were resuspended either for osmotic stabilization in SEM buffer (250 mM sucrose, 1 mM EDTA, and 10 mM MOPS [pH 7.2]) or for the destruction of the outer mitochondrial membrane in EM buffer (1 mM EDTA, and 10 mM MOPS [pH 7.2]). Mitochondrial membranes were disrupted by either 1% Triton X-100 for carbonate extraction experiments or by sonication for the detection of submitochondrial localization as a positive control.

QUANTIFICATION AND STATISTICAL ANALYSIS

Sample sizes were not a priori calculated. Data was analyzed using GraphPad Prism 8.0 (CA USA). All data is represented as mean ± SEM (standard error of mean) unless indicated otherwise. All replicates are biological unless indicated otherwise. All statistical tests are two-sided, only performed on raw data, and indicated in the respective figure legend for each dataset. In all panels: not significant, ns > 0.05; */†p<0.05; **/††p<0.01;***/†††p<0.001; ****/††††p<0.0001. For grooming behavior, the inter-rater reliability was determined by SPSS (IBM, CA USA). The inter-rater reliability is the degree of agreement among different independent raters and is expressed as Kappa. Kappa was interpreted according to guidelines from Cicchetti and Sparrow; (0.0=poor to 1.0=excellent) (Cicchetti and Sparrow, 1981). Five mice were excluded from the study because the sural nerve was touched – and potentially damaged – during the SNI surgery.

Cell Reports, Volume *37*

Supplemental information

Tmem160 contributes to the establishment of discrete nerve injury-induced pain behaviors in male mice

Daniel Segelcke, Hanna K. Fischer, Meike Hütte, Sven Dennerlein, Fritz Benseler, Nils Brose, Esther M. Pogatzki-Zahn, and Manuela Schmidt

Cell Reports, Volume *37*

Supplemental information

Tmem160 contributes to the establishment of discrete nerve injury-induced pain behaviors in male mice

Daniel Segelcke, Hanna K. Fischer, Meike Hütte, Sven Dennerlein, Fritz Benseler, Nils Brose, Esther M. Pogatzki-Zahn, and Manuela Schmidt

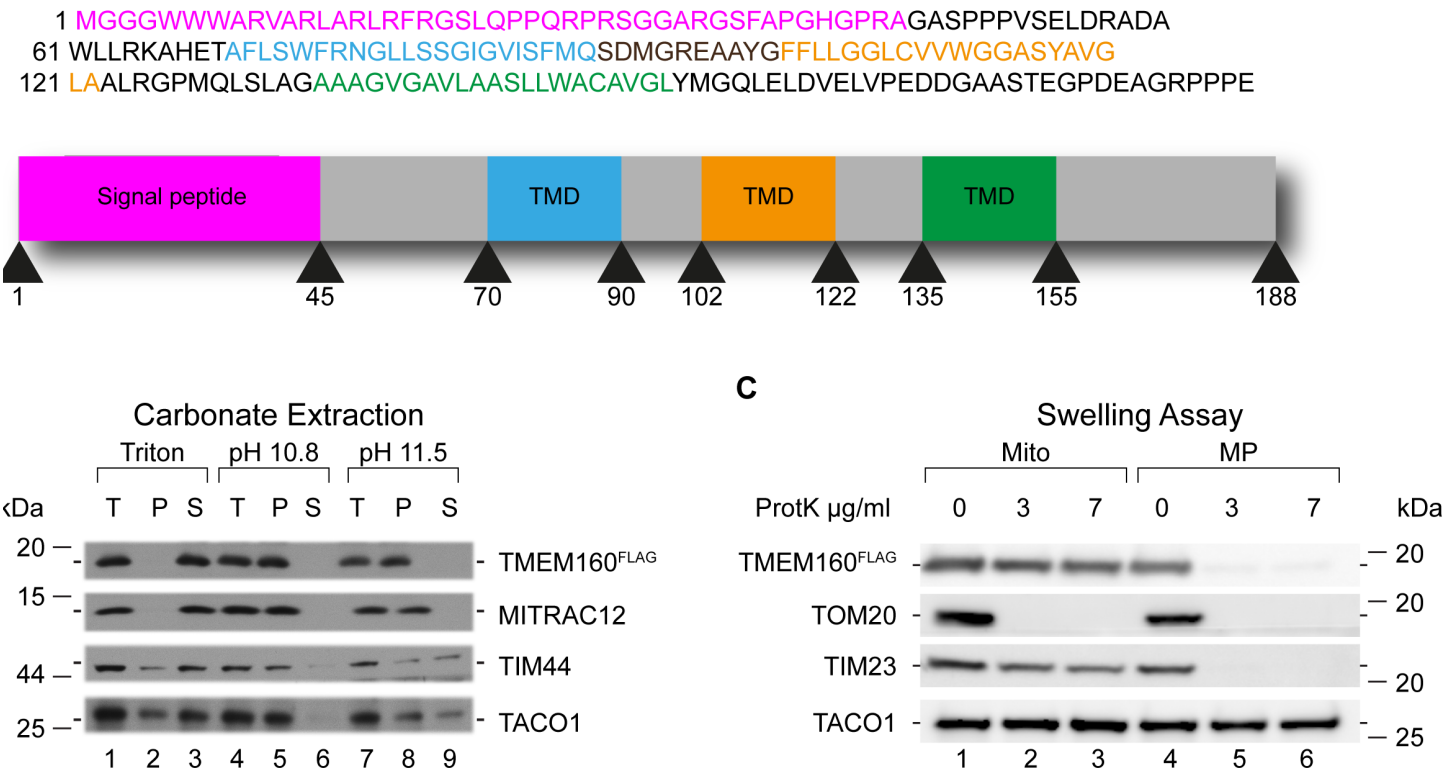

Figure S1: Tmem160 is localized to mitochondria, Related to Figure 1
(A) Tmem160 exhibits an N-terminal signal peptide (aa 1-45) for mitochondrial import (MitoProt II - v1.101, https://ihg.gsf.de/ihg/mitoprot.html) and 3 predicted transmembrane domains. **(B)** Submitochondrial location of Tmem160 was analyzed by carbonate extraction. Tmem160-Flag protein (Tmem160^{FLAG}) was transiently expressed in HEK293T cells. Isolated mitochondria were subjected to detergent lysis (Triton) or carbonate extraction at different pH (as indicated). MITRAC12 was used as a positive control for a membrane-integrated protein, while the membrane-associated TIM44 as well as the soluble TACO1 served as negative controls since they are known to dissociate from the inner mitochondrial membrane under higher pH-conditions. Tmem160-Flag was resistant to carbonate extraction suggesting its integration into mitochondrial membranes. (T = total; P = pellet, S = soluble fraction). N=2 independent mitochondria isolations. **(C)** Submitochondrial location of Tmem160 was analyzed by the "protease protection assay": Tmem160-Flag was transiently expressed in HEK293T cells and mitochondria isolated (Mito). Proteinase K (PK) was added to isolated mitochondria (Mito) and to hypotonically swollen mitochondria (swelling assay producing mitoplasts, MP) for 10 min. Probing for TOM20 served as a marker at the outer mitochondrial membrane, TIM23 served as a marker protein at the inner mitochondrial membrane, and TACO1 as a marker for the mitochondrial matrix. Accordingly, TOM20 signals disappeared upon PK treatment, while TIM23 was only accessible for PK upon hypo-osmotic swelling (in MP). As expected, the mitochondrial matrix marker TACO1 did not alter, even when the outer mitochondrial membrane was disrupted by PK treatment. Tmem160-Flag only became accessible to PK treatment in MP, i.e., when the outer mitochondrial membrane was disrupted by hypotonic swelling (similar to TIM23) indicative of its localization at the inner mitochondrial membrane. N=2 independent mitochondria isolations.

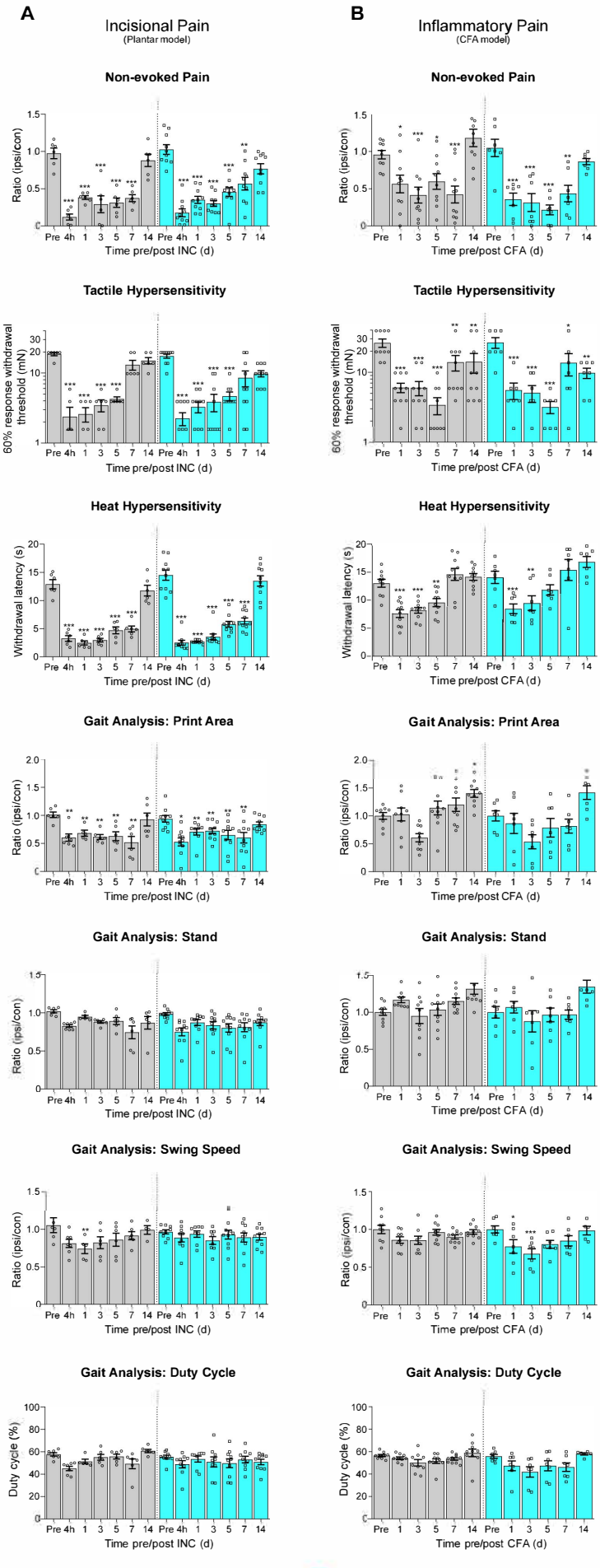
A
Incisional Pain
(Plantar model)
B
Inflammatory Pain
(CFA model)
Non-evoked Pain
Ratio (ipsi/con)
Time pre/post INC (d)
Time pre/post CFA (d)
Tactile Hypersensitivity
60% response withdrawal threshold (mN)
Heat Hypersensitivity
Withdrawal latency (s)
Gait Analysis: Print Area
Gait Analysis: Stand
Gait Analysis: Swing Speed
Gait Analysis: Duty Cycle
Duty cycle (%)
Pre 4h 1 3 5 7 14 Pre 4h 1 3 5 7 14
Pre 1 3 5 7 14 Pre 1 3 5 7 14
WT
Tmem160-/-

Figure S2: Raw data of behavioral assays in the plantar model of incisional pain and the CFA-model of inflammatory pain, Related to Figure 3

(A) Unilateral plantar incision induced non-evoked pain behavior, tactile, and heat hypersensitivity. Moreover, gait analysis showed the expected reduction of the print area during movement while other measured parameters were largely unchanged. No differences could be discerned between Tmem160$^{-/-}$ mice compared to WT littermates. N=6 (WT) and N=10 (Tmem160$^{-/-}$) mice. **(B)** Unilateral injection of complete Freund‘s adjuvant (CFA) into one hindpaw induced non-evoked pain behavior, tactile, and heat hypersensitivity. Howe-ver, gait analysis was largely unchanged. No differences could be discerned between Tmem160$^{-/-}$ mice compared to WT littermates. N=10 (WT) and N=7 (KO). Data are represented as mean ± SEM in a scatter bar plot. 2-way ANOVA Holm-Sidak‘s multiple comparison tests. * for comparison relative to pre-values. P-Values: * ≤ 0.05, ** ≤ 0.01, *** ≤ 0.001.

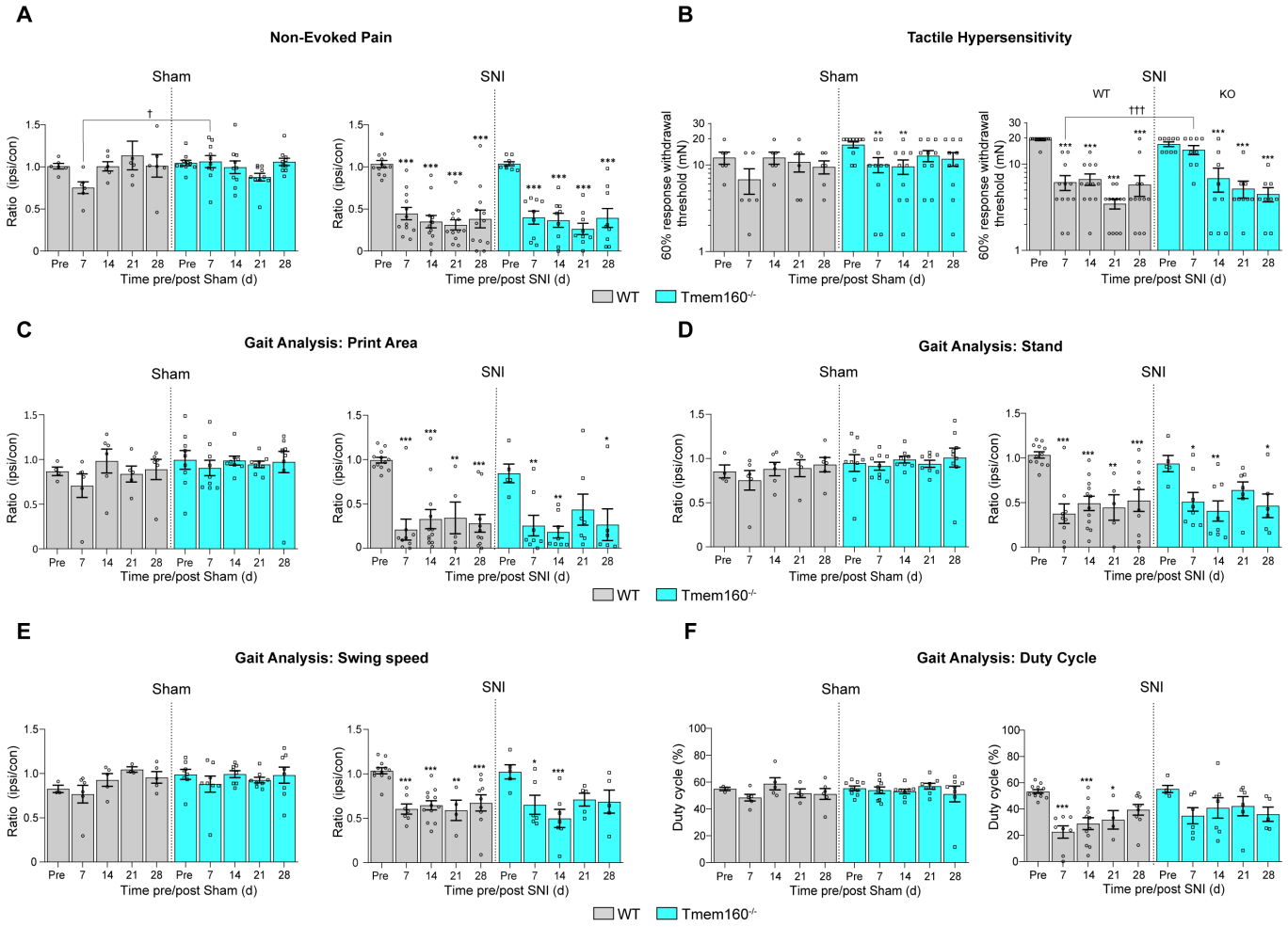

Figure S3: Raw data of behavioral assays in the spared nerve injury (SNI) model of neuropathic pain and sham-operated controls, Related to Figure 3

(A-F) No pain-related behavior was observed in Sham-operated mice in either genotype, except for non-evoked pain at 7d (A). Unilateral spared nerve injury (SNI) induced non-evoked pain behavior **(A)**, tactile hypersensitivity **(B)**, and alterations in static **(C, D)** and dynamic **(E, F)** gait parameters in WT littermates and Tmem160$^{-/-}$ mice. No difference among genotypes could be discerned with the exception of the delayed establishment of tactile hypersensitivity (i.e. strongly attenuated tactile hypersensitivity at 7d after SNI, as shown in Figure 3D) in Tmem160$^{-/-}$ mice. Sham: N=6 (WT) and N=9 (Tmem160$^{-/-}$) mice; SNI: N=12 (WT) and N=9 (Tmem160$^{-/-}$) mice. Data are represented as mean ± SEM in a scatter blot. Two-way ANOVA followed by Holm-Sidak's multiple comparison tests. * for comparison relative to pre-values. † for comparison between genotypes. P-Values: */†≤ 0.05, **/††≤ 0.01, ***/†††≤ 0.001.

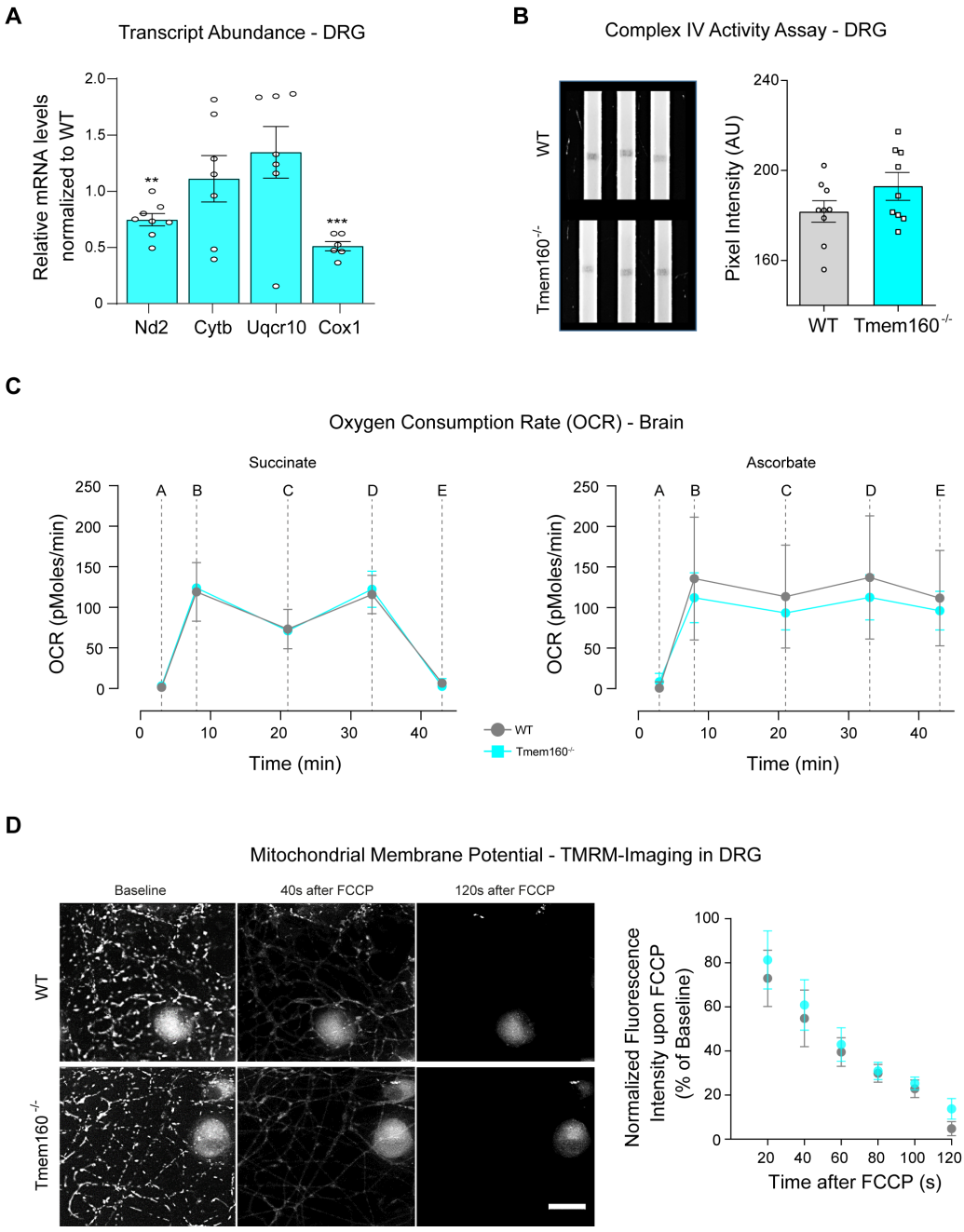

Figure S4: Mitochondrial function appears to be unaffected by *Tmem160* deficiency, Related to Figure 4
(A) Normalized transcript levels of several mitochondrial proteins in lDRG of Tmem160$^{-/-}$ mice relative to WT littermates as measured by qPCR. Mildly reduced transcript levels of several components of the electron transport chain (ETC) in DRG of Tmem160$^{-/-}$ mice were observed. Data are represented as mean ± SEM in a scatter bar plot. One-sample t-tests against a hypothetical value of 1.0 (i.e. normalized to WT littermates). P-Values: ** ≤ 0.01, *** ≤ 0.001. N=4-7 (WT) and N=6-8 (Tmem160$^{-/-}$). **(B)** Enzyme activity dipsticks for cytochrome c oxidase (COX, Complex IV) revealed no difference of COX activity in DRG lysates (both lDRG and total DRG) of Tmem160$^{-/-}$ and WT mice. (left) Representative images of 3 technical replicates of dipsticks in each genotype, and (right) quantification (depicted as Pixel intensity) across all experiments. Data are represented as mean ± SEM in a scatter bar blot. Unpaired student's t-test, ns. N=6 in 3 independent experiments with DRG of 2 mice/genotype/experiment; 3 technical replicates/genotype/experiment. **(C)** Oxygen consumption rate of isolated mitochondria from brains of WT and Tmem160$^{-/-}$ mice after incubation with succinate (left, a substrate for complex II) or ascorbate (right, a substrate for complex IV). No apparent functional alterations could be observed in Tmem160$^{-/-}$ mice compared to WT littermates. Within each graph: A, calibration; B, substrate (basal respiration); C, Oligomycin (ATP-linked respiration + proton leak); D, FCCP (maximal respiratory capacity); E, Antimycin A + Rotenone + KCN (spare reserve capacity). Data are represented as mean ± SEM. 2-way ANOVA followed by Holm-Sidak's multiple comparison tests, ns. N = 2-3 mice/genotype in 3 independent experiments. **(D)** TMRM imaging to monitor the mitochondrial membrane potential upon addition of FCCP. (left) Representative images of the TMRM signal at baseline and two time points after FCCP addition in DRG cultures of either genotype. (right) Quantification of the TMRM signal normalized to the baseline intensity for each genotype. Time course shows the expected decay of the TMRM signal upon FCCP addition. No apparent differences could be observed in Tmem160$^{-/-}$ mice compared to WT littermates. Data are represented as mean ± SEM. Scale bar, 20 µm; 2-way ANOVA followed by Holm-Sidak's multiple comparison tests, ns. Several coverslips from N=3 mice/genotype for n=3 independent cultures.

A

	1	2	3	4	5	6	7	8	9	10	11	12	13	14	15	16	17	18	19	20	21	22	23	24
A	Ref	Ref																					Ref	Ref
B	CXCL13	CXCL13	C5	C5	G-CSF	G-CSF	GM-CSF	GM-CSF	CCL1	CCL1	CCL11	CCL11	sICAM-1	sICAM-1	IFN-γ	IFN-γ	IL-1α	IL-1α	IL-1β	IL-1β	IL-1ra	IL-1ra	IL-2	IL-2
C	IL-3	IL-3	IL-4	IL-4	IL-5	IL-5	IL-6	IL-6	IL-7	IL-7	IL-10	IL-10	IL-13	IL-13	IL-12 p70	IL-12 p70	IL-16	IL-16	IL-17	IL-17	IL-23	IL-23	IL-27	IL-27
D	CXCL10	CXCL10	CXCL11	CXCL11	CXCL1	CXCL1	M-CSF	M-CSF	CCL2	CCL2	CCL12	CCL12	CXCL9	CXCL9	CCL3	CCL3	CCL4	CCL4	CXCL2	CXCL2	CCL5	CCL5	CXCL12	CXCL12
E	CCL17	CCL17	TIMP-1	TIMP-1	TNF-α	TNF-α	TREM-1	TREM-1																
F	Ref	Ref																					PBS	PBS

B

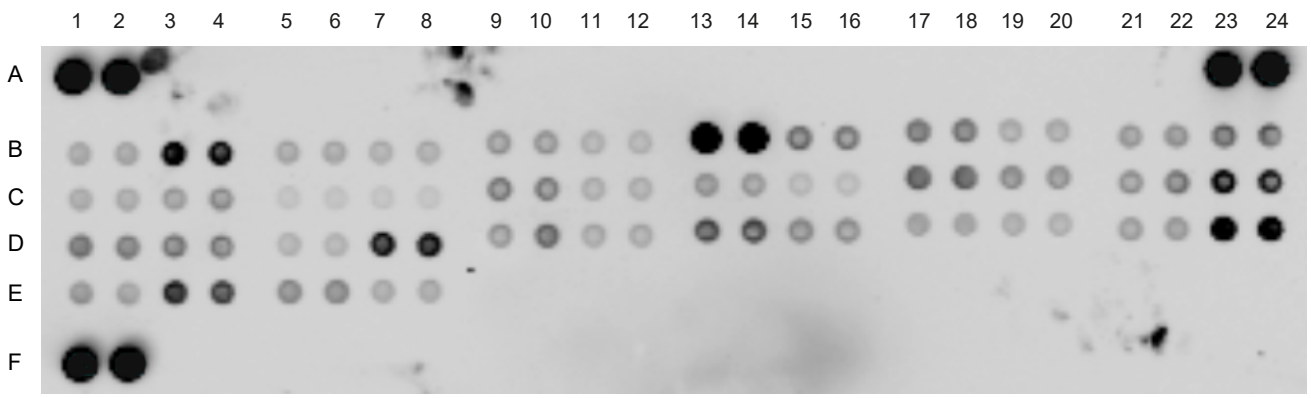

Figure S5: Cytokine Array: panel coordinates and raw image, Related to Figures 4 and 5
(A) Panel coordinates as given by the manufacturer. **(B)** Exemplary original image of a membrane in Figure 4 (male Tmem160$^{-/-}$).

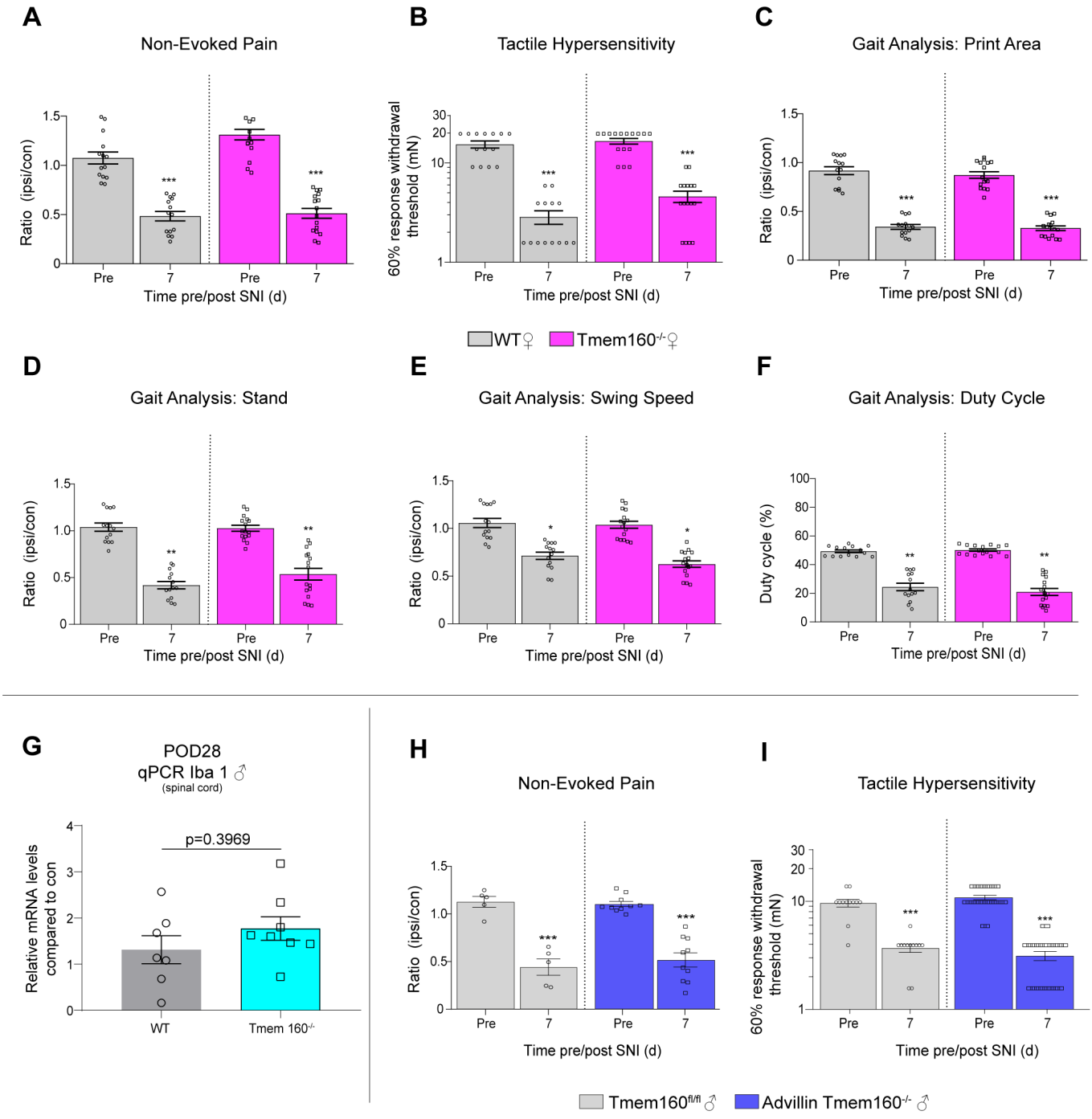

Figure S6: Raw data of behavioural assays in the SNI model of neuropathic pain and *Iba1*-levels 28d post SNI, Related to Figures 4 and 5

(A-F) Female global KO mice: Unilateral spared nerve injury (SNI) induced non-evoked pain behavior (A), tactile hypersensitivity (B), and alterations in static (C, D) and dynamic (E, F) gait parameters in female WT littermates and female global KO mice. No difference among genotypes could be discerned. N=14 (WT) and N=16 (Tmem160$^{-/-}$) mice. **(G)** 28d post SNI *Iba1* mRNA levels were similarly upregulated in the ipsilateral spinal cord (compared to the contralateral side) in male WT and global KO mice. Data are depicted as mean ± SEM in a scatter bar plot. Mann-Whitney test between genotypes, p = 0.39, ns. N=7 (WT) and N=8 (Tmem160$^{-/-}$) mice. **(H-I)** Male Advillin-Cre Tmem160$^{-/-}$ (cKO) mice: Unilateral spared nerve injury (SNI) induced non-evoked pain behavior (H) and tactile hypersensitivity (I) in both floxed littermate controls (Tmem160$^{fl/fl}$) and cKO male mice. (H) N=5, Tmem160$^{fl/fl}$; N=10, Advillin Tmem160$^{-/-}$. (I) N=12 Tmem160$^{fl/fl}$; N=22, Advillin Tmem160$^{-/-}$.

(A-F, H, I) Data are represented as mean ± SEM in a scatter bar blot. 2-way ANOVA followed by Holm-Sidak's multiple comparison tests. * for comparison relative to pre-values. P-Values: *≤ 0.05, **≤ 0.01, ***≤ 0.001.

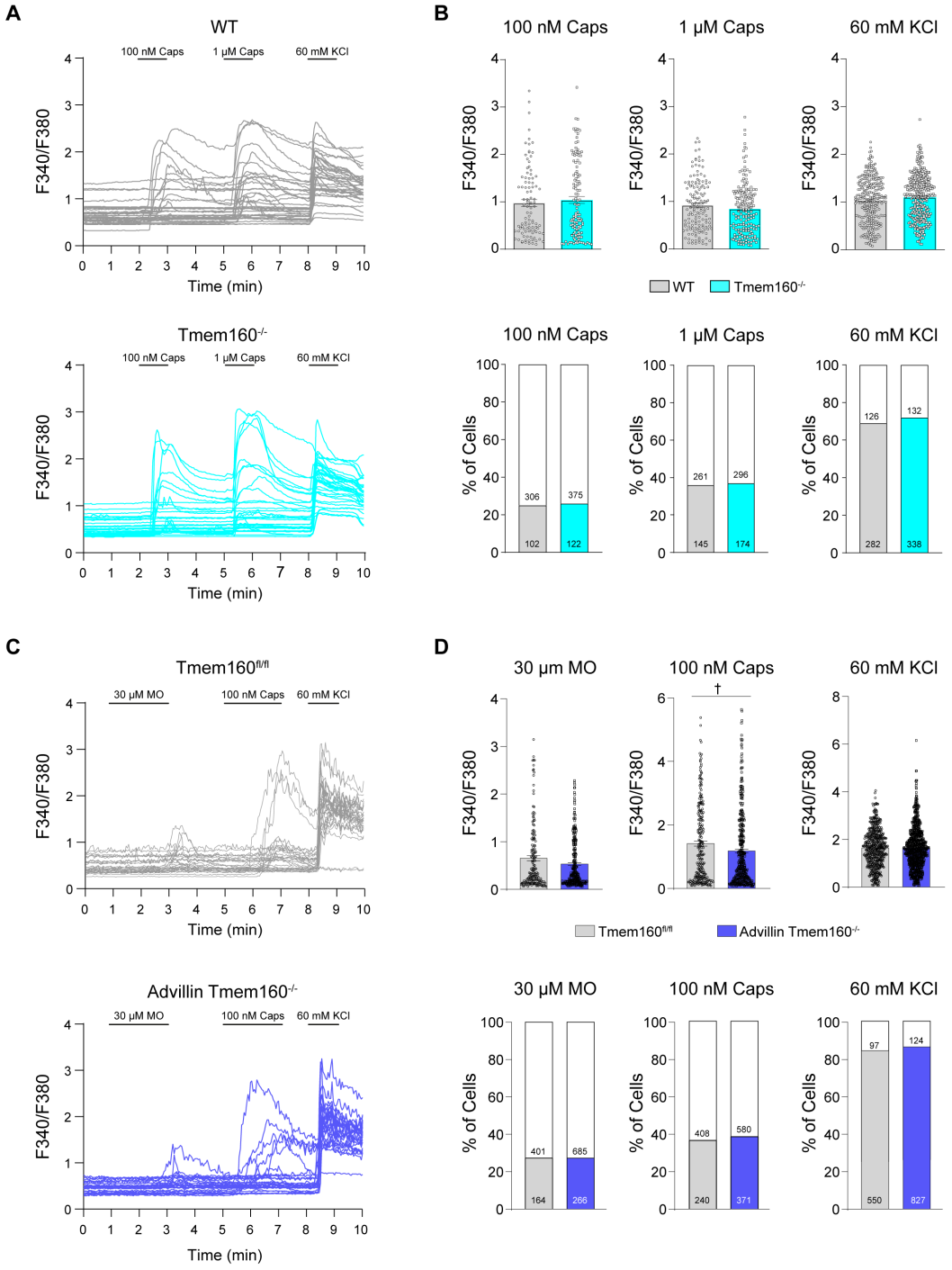

Figure S7: Tmem160 does not affect TRPV1-mediated neuronal activity and possibly exerts its major role in non-neuronal cells, Related to Figure 7

(A-B) Ratiometric Ca^{2+}-Imaging was performed in cultured DRG neurons of naïve Tmem160$^{-/-}$ and WT males. Representative traces and stimulation protocol are indicated by black horizontal bars (A). No significant differences in response amplitudes (B, top) and percentage of responding (colored part) neurons (B, bottom) could be discerned among genotypes. The total number of neurons assessed is depicted in the respective bars (B, bottom). Data are represented as mean ± SEM in a scatter bar plot (B, top) or as percentage of responding versus non-responding neurons (B, bottom). Mann-Whitney Test (B, top) and Fisher's exact test (B, bottom), both ns for comparison between genotypes. Multiple coverslips from N=3 mice/genotype were imaged.

(C-D) Ratiometric Ca^{2+}-Imaging was performed in cultured DRG neurons of cKO males (Advillin-Cre Tmem160$^{fl/fl}$) and male Tmem160$^{fl/fl}$ littermates. Representative traces and stimulation protocol are indicated by black horizontal bars (C). With the exception of a mild decrease of response amplitudes to Caps in cKO, no major differences in response amplitudes (D, top) and percentage of responding (colored part) neurons (D, bottom) could be discerned among genotypes. The total number of neurons assessed is depicted in the respective bars (D, bottom). Data are represented as mean ± SEM in a scatter bar plot (D, top) or as percentage of responding versus non-responding neurons (D, bottom). Mann-Whitney Test (D, top) and Fisher's exact test (D, bottom), † $p \leq 0.05$ and ns for comparison between genotypes. Multiple coverslips from N=3 mice/genotype were imaged.

Table S1: Oligonucleotide information, Related to STAR Methods

	Forward (always 5'-3')	Reverse (always 5'-3')
GAPDH	CAATGAATACGGCTACAGCAAC	TTACTCCTTGGAGGCCATGT
Iba-1	GGATTTGCAGGGAGGAAAA	TGGGATCATCGAGGAATTG
mt-Cox1	GAACCCTCTATCTACTATTCGG	CAAGTCAGTTTCCAAAGCCT
mt-Cytb	ATTCCTTCATGTCGGACGAG	GGGATGGCTGATAGGAGGTT
mt-ND2	CGCCCCATTCCACTTCTGATTACC	TTAAGTCCTCCTCATGCCCCTATG
Tmem160	TCTCCTTCATGCAGAGTGACAT	ATCCTCAGGCACCAGTTCCAC
Uqcr10	CGCAGAACTTCCACCTTTGC	CCACAGTTTCCCCTCGTTGA
Genotyping Primer (always 5'-3')		
Advillin-Cre genotyping **Fragment size: 281 bp**		TTTCCGGTTATTCAACTTGCACCA GCAATGGCTCCCTGTTCACT
Tmem160 genotyping **Fragment sizes: *Tmem160 WT* = 235 bp; *Tmem160 floxed* = 269 bp; *Tmem160 recombined, KO* = 202 bp**		ACTAGTACAAGTTTTGTTTCCTGGC GGCCAGAGTAAGGCAAGCATC CGGTCTCTCACCTAGGCAGT